

The influence of near surface sediment hydrothermalism on the TEX₈₆ tetraether lipid-based proxy and a new correction for ocean bottom lipid overprinting

Jeremy N. Bentley^a, Gregory T. Ventura^a, Clifford C. Walters^b, Stefan M. Sievert^c, Jeffrey S. Seewald^c

^a Department of Geology, Saint Mary's University, Halifax, Nova Scotia B3H 3C3, Canada.

^b Bureau of Economic Geology, University of Texas at Austin, USA.

^c Woods Hole Oceanographic Institution, Woods Hole, USA.

* Corresponding author: Todd.ventura@smu.ca

For submission to: *Biogeosciences*

Number of pages: 32

Number of Figures: 6

Number of Tables: 2

Supplementary pages: 6

Key Points

- High *i*GDGTs turnover in shallow sediments is shown to be non-selective and does not impact TEX₈₆ paleoclimate ratios.
- The proxy nonetheless can be overprinted by addition of sediment sourced lipids when geothermal temperatures rise above ~60–70 °C.
- A universally applicable, diagenetic correction model is presented to remove overprinting artifacts in the TEX₈₆ proxy.

Abstract

The diversity and relative abundances of tetraether lipids produced by Thaumarchaeota in soils and sediments increasingly is used to assess environmental change. For instance, the TetraEther indeX of 86 carbon atoms (TEX₈₆), based on archaeal isoprenoidal glycerol dialkyl glycerol tetraether (*i*GDGT) lipids, is frequently applied to reconstruct past sea-surface temperatures (SST). Yet, it is unknown how the ratio fully responds to environmental and or geochemical variations and if the produced signals are the adaptive response by Thaumarchaeota to climate driven temperature changes in the upper water column. We present the results of a four push-core transect study of surface sediments collected along an environmental gradient at the Cathedral Hill hydrothermal vent system in Guaymas Basin, Gulf of California. The transect crosses a region where advecting hydrothermal fluids reach 155 °C within the upper 21cm below the seafloor (cmbsf) close to the vent center to near ambient conditions at the vent periphery. The recovered *i*GDGTs closest to the vent center experienced high rates of turnover with up to 94% of the lipid pool being lost within the upper 21 cmbsf. Here, we show that the turnover is non-selective across TEX₈₆ GDGT lipid classes and does not independently affect the ratio. However, as evident by TEX₈₆ ratios being highly correlated to the Cathedral Hill vent sediment porewater temperatures ($R^2 = 0.84$), the ratio can be strongly impacted by the combination of severe lipid loss when it is coupled to the addition of *in situ* *i*GDGT production from archaeal communities living in the vent sediments. The resulting signal overprint produces absolute temperature offsets of up to 4 °C based on the TEX₈₆^H -calibration relative to modern climate records of the region. The overprint is also striking given the flux of GDGTs from the upper water column that is estimated to represent ~93% of the combined intact polar lipid (IPL) and core GDGT lipid pool initially deposited on the seafloor. A model to correct the overprint signal using IPLs is therefore presented that can similarly be applied to all near-surface

marine sediment systems where calibration models or climate reconstructions are made based on the TEX₈₆ measure.

1. Introduction

Archaeal and bacterial tetraether cellular membrane lipids mark-represent a group of common and structurally diverse compounds that are frequently used to track the presence of living and dead microorganisms as well as geochemical and physical conditions within in-the-geosphere-present day and paleoenvironments -(e.g. Schouten et al., 2002, 2004; 2013-; 2004; Hopmans et al., 2004; Weijers et al., 2007, 2014; Hollis et al., 2012; Peneost-Lipp et al., 2008REFsO'Brien, et al., 2017; Stuart et al., 2017). The-In this regard, the proportional abundances of these lipids formsform various prominent proxies for assessing environmental change through time. For example, TEX₈₆ (TetraEther indeX with 86 carbon atoms; -(Schouten et al., 2002) is the most widely used archaeal lipid-based paleotemperature proxy for marine environments (Table 1; Eq. 1). This proxyThe ratio measures variations in the number of cyclopentyl rings within the hydrocarbon skeleton offor a select range-group of archaeal core lipids (CLs) elasses (Supplementary Figure A-1) following -following the initial assumption that biphytanyl cyclization of-the-biphytanyl-moiety-is an organismal response to changing sea surface temperatures (SSTs). The proxy is therefore used in paleo-oceanographic studies in many different regions around the world (e.g. Huguet et al., 2006; Kim et al., 2008; McClymont et al., 2012; Tierney, 2014) with TEX₈₆ values typically ranging from 0.2–0.9 in both marine and lake sediment (Sinninghe Damsté et al., 2009; Powers et al., 2010; Zhang et al., 2016; Morrissey et al., 2018; Yao et al., 2019; Kumar et al., 2019). The utility of TEX₈₆ rests on the premise that isoprenoidal GDGTs (-iGDGTs) found in ocean bottom sediments are almost exclusively produced by marine planktonic Thaumarchaeota-archaea that inhabit the epipelagic zone (Wakeham et al., 2003; Tierney, 2014; Blessing et al., 2019, 2020; REFsRoger Summons PNAS-paper). TEX₈₆-based lipids are therefore required to be efficiently and continually transported from the upper water column to the underlying ocean floor sediments to produce a chemostratigraphic record of microbial response to changing SST conditions (Wuchter et al., 2005).

Since its introduction, the reliability of TEX₈₆ to accurately track paleoclimate variations has been questioned. TEX₈₆-based SST estimates have been observed to substantially deviate from other temperature proxies (e.g., Huguet et al., 2006; Rommerskirchen et al., 2011; Seki et al., 2012). For-For example, over the past decade, considerable effort has been made to reconstruct the early Paleogene greenhouse climate with a variety of paleoclimate proxies (Hollis et al., 2012). However, TEX₈₆ appears to significantly over-estimate reconstructed SSTs relative to other proxies such as Mg/Ca, clumped isotopic compositions of foraminiferal calcite, as well as various climate models based on partial pressure of carbon dioxide ($p\text{CO}_2$) predictions (Lunt et al., 2012; Naafs et al., 2018). For late Neogene climate reconstructions, the proxy has been shown to underestimate warming trends relative to U_{37}^K -derived temperatures (Lawrence et al., 2020). The apparent offsets in SST reconstructions have been attributed to complications arising from a lack of understanding on how the proxy's associated lipids change in relation to their environment and if these changes are regulated by internal adaptations within the archaeon or by an overarching community succession.

In this regard, the debate surrounding these offsets largely centers on establishing responses to seasonal biases (e.g. REFsHerford et al., 2006; Wuchter et al., 2006; Huguet et al., 2011); the development of The apparent high SST reconstructions have been attributed to proxy complications including adequate calibration methods (e.g. Kim et al., 2010; Pearson et al., 2013; Tierney et al. 2014); identifying lipid sourcing effects – eeanincluding -subsurface sediments origins for those used with the calculation of TEX₈₆ lipids (e.g. Lipp and Hinrichs, 2009; Ho and Laepple, 2016)-; or byas the result of physical, chemical, and ecological controls on archaeon iGDGTs cyclization (e.g. Elling et al., 2015; Qin et al., 2015; Hurley et al., 2016).

For the various non-thermal influences, the primary concern has been what archaeal taxa produce iGDGTs and where are they sourced in the water column. To this end, For late Neogene climate reconstructions, the proxy has been shown to underestimate warming trends relative to U_{37}^K -derived temperatures (Lawrence et al., 2020). In this regard, the debate largely centers on a lack of understanding of how the proxy's associated

Formatted: Not Highlight

Formatted: Not Highlight

Formatted: Not Highlight

Formatted: Not Highlight

Formatted: Subscript

Formatted: Font: Italic

lipids precisely change in relation to their environment and if these changes are regulated by internal adaptations within the archaeon or by community succession (Elling et al., 2015; Qin et al., 2015)

most TEX₈₆-based lipids are thought to be sourced from Marine Group I (MGI) planktonic Thaumarchaeota (Brochier-Armanet et al., 2008), which are most abundant below the photic and epipelagic zone (e.g. Karner et al., 2001) with potentially some inputs from Marine Group II (MGII), Euryarchaeota, that live in the upper 100 m of the water column (Lincoln et al., 2014; Wang et al., 2015; Ma et al., 2020). Studies from the Pacific Ocean (Karner et al., 2001; Pearson et al., 2013) and Southern Atlantic (Hurley et al., 2016) have shown that peak archaeal abundances occur at 100–350 m depth. ~~And the TEX₈₆ lipids should therefore not produce a direct response to changing SSTs.~~ To address the impact of depth habitat, Schouten *et al.* (2013) proposed a calibration based on suspended particulate matter and *in situ* water temperature from the upper 100 m of the global ocean. In this regard, ocean floor sediment measured TEX₈₆ values may become highly impacted by the collection of mixed source inputs from the colder, deeper water column. Evidence of this has been provided by a strong positive correlation between water depth and differences in TEX₈₆^H values as observed in both surface sediments and suspended particulate organic matter from the Mediterranean Sea (Kim et al., 2015). Here the TEX₈₆ dissimilarities appear to be driven by increases in the relative abundances of GDGT-2 and the isomers of crenarchaeol (see Lui et al., 2018; Sinninghe Damsté et al., 2018) coupled to decreasing abundances of GDGT-1 and GDGT-3 with deeper water depths. Collectively this produces a systematic reconstructed SST bias for deep-water surface sediments. Such sourcing effects have therefore further resulted in speculation that the TEX₈₆ ratio of open ocean sediments may actually reflect deeper water column and subsurface rather than SSTs (Huguet et al., 2007; Lopes dos Santos *et al.*, 2010; Kim *et al.*, 2012a,b; Ho & Laepple, 2016; Hurley et al., 2016). To compensate for this, both TEX₈₆^H and TEX₈₆^L have been re-calibrated against subsurface (0–900 m water depth) temperatures (Kim *et al.*, 2012a,b; Ho & Laepple, 2016). Other non-thermogenic driving forces impacting the production, cyclization, and relative abundance of TEX₈₆-based lipids include organismal selectivity to specific growth phases and growth rates (Elling et al., 2014; Hurley et al., 2016); and redox conditions (Qin et al., 2015).

~~Non-thermal influence resulting from lipid abundances being brought to marine sediments from non-planktonic Thaumarchaeota origins such as from the deep water or within marine sediments (Liu et al., 2011).~~

Additionally, most Thaumarchaeota are found below the photic and epipelagic zone ~~and should therefore not produce a direct response to changing SSTs.~~ Studies from the Pacific Ocean (Karner et al., 2001; Pearson et al., 2013) and Southern Atlantic (Hurley et al., 2016) have shown that peak archaeal abundances occur at 100–350 m depth (Karner et al., 2001; Pearson et al., 2013). To address the impact of depth habitat, Schouten *et al.* (2013) further proposed a calibration based on suspended particulate matter and *in situ* water temperature from the upper 100 m of the global ocean. In this regard, if these deeper sourced lipids are deposited on the seafloor than the sedimentary GDGT used to generate sea surface temperatures are mixed ~~mixes with comprising of significant contributions from much colder waters.~~ ocean floor sediment measured ~~potentially impacting the reconstructed values providing much lower SSTs.~~ As TEX₈₆ values may therefore become disproportionality highly impacted by the collection of mixed source inputs, the location of lipid loading from the deeper water column to the ocean floor sediments. Evidence of this has been provided by a seems to be an factor as strong positive correlationrelationship between water depth and differences in TEX₈₆^H values are ~~as~~ observed in both surface sediments and suspended particulate organic matter from the Mediterranean Sea (Kim et al., 2015). The Here the TEX₈₆ differencesdissimilarities appear to be driven by increases in the relative abundances of GDGT-2 and the isomers of crenarchaeol. TEX₈₆ lipids GDGT-2 and the isomers of crenarchaeol (Lui et al., 2018; Sinninghe Damsté et al., 2018) coupled to decreasing abundances of GDGT-1 and GDGT-3 with increasing deeper water depths. The ~~thereby producing a systematic reconstructed SST bias~~ systematic change results in a higher reconstructed SST bias for deep-water surface sediments. Therefore, such sourcing effects have further resulted in speculation that the TEX₈₆ ratio of open ocean sediments may actually reflect deeper water column and subsurface rather than that of SSTs (Huguet et al., 2007; Lopes dos Santos *et al.*, 2010; Kim *et al.*, 2012a,b; Ho & Laepple, 2016; Hurley et al., 2016). To compensate for this, both TEX₈₆^H and TEX₈₆^L have been re-calibrated against subsurface (0–900 m water depth) temperatures (Kim *et al.*, 2012a,b; Ho & Laepple, 2016).

Formatted: Subscript

Formatted: Subscript

Formatted: Not Highlight

Formatted: Not Highlight

The *i*GDGT relative abundances recorded in a TEX₈₆ measurements may constitute a multi-variable system, having both a component of lipids contributed to the “pool” via *in situ* sources and by depositional processes. TEX₈₆-based SST estimates have been observed to substantially deviate from other temperature proxies (e.g., Huguet et al., 2006; Liu et al., 2009; Rommerskirchen et al., 2011; Hollis et al., 2012; Seki et al., 2012) implying these values can be a response to seasonal biases, non thermal influences, or other ecological signals.

Non-thermal influence result from lipid abundances being brought to marine sediments from non-planktonic Thaumarchaeota origins such as from the deep water or within marine sediments (Liu et al., 2011; Kerou et al., 2020).

There are likely other driving forces other than temperature that impact the archaeal GDGT production and relative abundances. Some examples of these drivers include organismal selectivity to specific growth phases and growth rates (Elling et al., 2014; Hurley et al., 2016); ammonia oxidation rates (Hurley et al., 2016); and redox conditions (Qin et al., 2015).

By artificially hydrolyzing the headgroups of marine archaeal IPLs harvested from a sediment trap, Lipp and Hinrichs (2009) demonstrated that the production of IPL-GDGTs by ocean floor sediment microbial communities collected in the Peru Margin were distinctly different from upper water column sourced CLs and that the conversion of this living pool to a fossil pool of lipids would shift TEX₈₆ ratios to higher values, may impact TEX₈₆ values. Similarly, Elling et al. (2013) confirmed TEX₈₆ values can represent a mixed GDGT signal from both active microbial production in shallow sediments and fossil lipids sourced from the water column. These authors further demonstrated that TEX₈₆ values from cultures can diverge from the global calibration that forms the basis for most climate reconstructions suggesting that the sedimentary community compositions may exert some controls on the TEX₈₆ signal. Elling et al. (2013) further extended these concerns, suggesting TEX₈₆ reflects subsurface temperatures rather than SSTs as the input of GDGTs in marine settings are not exclusive to Thaumarchaeota, because a majority of marine group I (MGI) Archaea also reside in subsurface waters or marine sediments. Collectively, these observations indicate a sub-pelagic zone where microorganisms may mix with the GDGTs from the surface, thus providing mixed signals and inaccurate TEX₈₆ values from mixed sources. However, other authors have found that TEX₈₆ ratios are not impacted by benthic Archaea due to the low relative turnover rates for the lipids in marine sediments (Lengger et al., 2012, 2014; Omuh Umoh et al., 2020). Omuh Umoh et al. (2020) found little effect to the TEX₈₆ paleoclimate ratio when examining surface sediments near hydrothermal vent sites on the Southeast Indian Ridge in the southern Indian Ocean. Lengger et al. (2012, 2014) reported no significant deviation between the TEX₈₆ values in sediment cores collected near the oxygen minimum zone from that of the overlying water column in the Arabian Sea with near linear degradation rates of both IPLs and CLs.

All together, the *i*GDGT relative abundances recorded in a sediment TEX₈₆ measurement may ultimately constitute a multi-variable datapoint, mixing lipid components that are themselves responses to temperature, organismal substrate and metabolism dynamics, and biozone niche partitioning that spans from the ocean surface to *in situ* shallow sediment community pools lastly further attenuated by depositional and diagenetic processes.

While not an ideal location to create SST reconstructions, hydrothermal vents of sedimented ocean basins do represent an anomalous end-member to the vast expanse of ambient ocean floor sediment where paleoclimate reconstructions are commonly produced. The Guaymas Basin, Gulf of California (Figure 1) is one such site. The basin experiences elevated sedimentation rates ranging between 0.4–0.2 cm yr^{-1} (Curry et al., 1979; Gieskes et al., 1988) due in part to the high productivity of the upper water column. The ocean floor hydrothermally impacted surface sediments are also a location of active and diverse microbial communities with vents that are often covered by Beggiatoa dominated microbial mats (e.g. McKay et al., 2012; Meyer et al., 2013; Teske et al., 2016). These sites should in principle, enable a high-resolution archaeal lipid-based paleoclimate stratigraphic record that provides optimal conditions for studying potential shallow diagenetic and subsurface subsurface lipid overprinting or interferences to common archaeal lipid-based environmental proxies. Recently, Bentley et al. (2022) produced a survey of the source and diagenetic and catagenetic alteration of archaeal lipids from the Cathedral Hill hydrothermal vent complex (Figure 1) in the Guaymas Basin, Gulf of California. Within that investigation, it was observed that most *i*GDGTs were sourced from the overlying water column. It was also observed that these lipids can become heavily turned over in the hotter portions of the vent site where they rarely survive long enough to become cracked into hydrocarbon

Formatted: Not Highlight

Formatted: Font color: Text 1, Not Highlight

Formatted: Font color: Text 1

Formatted: Font color: Text 1, Not Highlight

Formatted: Font color: Text 1

Formatted: Font color: Text 1, Not Highlight

Formatted: Font color: Text 1, Subscript, Not Highlight

Formatted: Font color: Text 1, Not Highlight

Formatted: Not Highlight

Formatted: Superscript

Formatted: Not Highlight

Formatted: Not Highlight

Formatted: Not Highlight

Formatted: Not Highlight

Formatted: Font: Italic

biomarkers such as biphytanes and derivatives of biphytanes. For this study, we further examine the *i*-GDGT lipid distributions in these near-surface ocean floor sediments from the Cathedral Hill hydrothermal vent complex (Figure 1) in the Guaymas Basin to determine if sea-surface paleoclimate proxy signals can be impacted by the presence of subsurface archaeal populations. The distribution of *i*-GDGTs and their corresponding environmental proxy signals were measured within the sediments along a transect at the Cathedral Hill hydrothermal vent system complex. In this regard, this site offers the unique opportunity to evaluate the response of TEX₈₆ and other tetraether-lipid proxies within a microbially diverse sedimentary environment that is exposed to high temperature vent fluids.

Formatted: Font: Italic

Formatted: Font: Italic

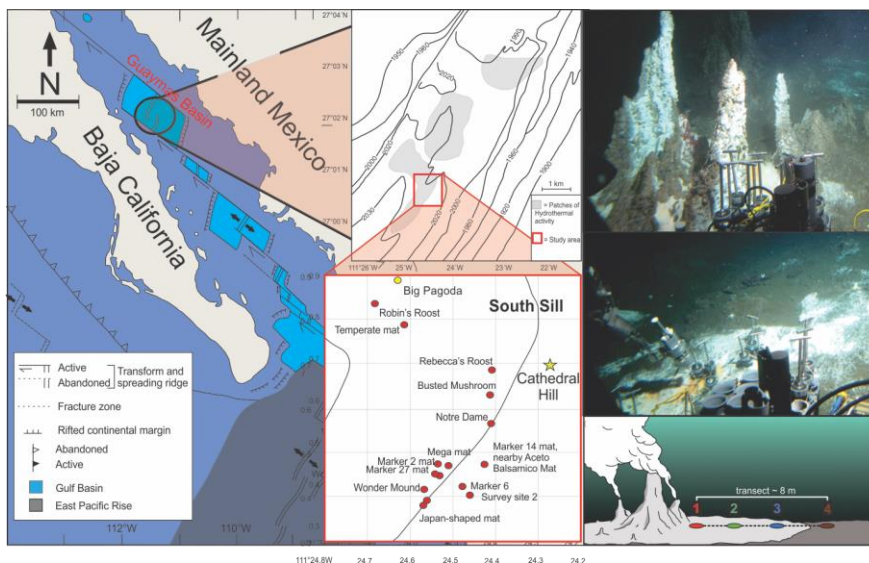
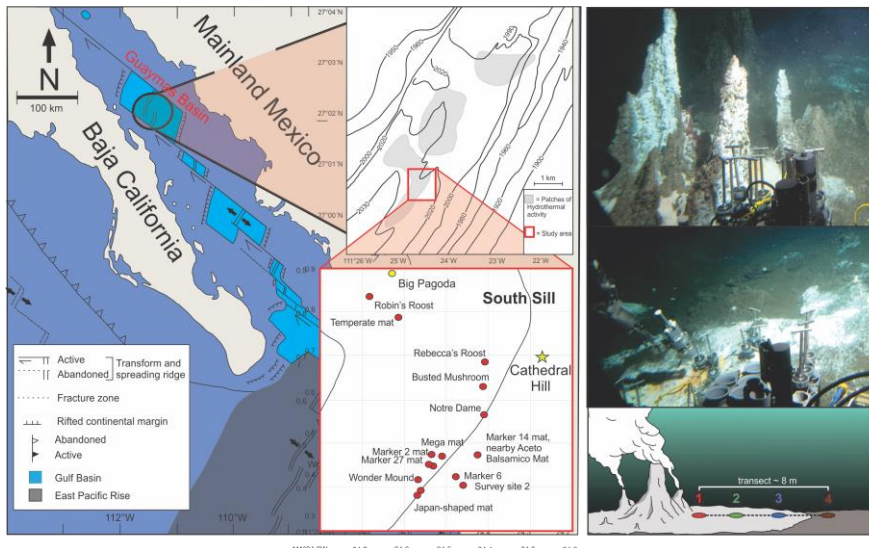


FIGURE 1 A) Location map of Guaymas Basin and the Southern Sill (red outlined box) in the Gulf of California. Cathedral Hill is marked with a yellow star. B) Photo of Cathedral Hill taken via *Alvin*. C) Schematic of the push core transect with a color-coding that is consistent for all plots throughout this paper. Maps modified from Teske et al. (2016), Dalzell et al. (2021), and Bentley et al. (2022).

Formatted: Not Highlight

Formatted: Not Highlight

Formatted: Not Highlight

236 2. Material and methods

237 2.1. Study location and sampling

238 Four sediment push cores were collected using HOV *Alvin* (Dive 4462; 10/22/08) at the Cathedral Hill
239 hydrothermal vent site, located at a water depth of 1996 m in the Southern Trough of Guaymas Basin, Gulf
240 of California (27°0.629' N, 111°24.265' W) (Figure 1). The push cores, labeled 1 to 4, were taken along a
241 transect with ~ 2 m spacing extending outwards from microbial mat-covered sediments near the sulfide
242 chimney complex to just outside of the microbial mat area in ambient seafloor sediment. Thermal-probe
243 measurements were sequentially taken ~~next-beside~~ each core (Table 1). Once the push cores were brought
244 to the surface, ~~they-the sediments~~ were subsampled into 2–3 cm-thick depth intervals, transferred to
245 combusted glass vials, and immediately stored at -40 °C (onboard the ship) before being shipped under dry
246 ice to the laboratory and later freeze-dried and stored at -80 °C ~~until being later processed~~.

263 Table 1. Sediment geochemical and lipid proxy data.

Core ^a	Depth interval (cmbsf)	Alvin dive # and core ID	Description/lithology ^b	Pore water temperature (°C)	Interpolated Pore water temperature (°C)	Sediment weight (g)	TLE sed
1	0-2	GB4462-5	Black mud with microbial mat filaments	19	19	1.97	11.5
1	2-4	GB4462-5	Brownish-green diatomaceous mud	-	67	2.04	7.65
1	4-6	GB4462-5	Brownish-green diatomaceous mud	85	85	2.03	9.37
1	6-8	GB4462-5	Brownish-green diatomaceous mud	-	105	1.99	2.09
1	8-10	GB4462-5	Brownish-green diatomaceous mud	-	117	2.01	4.38
1	10-12	GB4462-5	Grayish-green mud	121, 124	125	2.01	1.97
1	12-15	GB4462-5	Brownish-green consolidated mud with clay shards	-	135	1.98	1.99
1	15-18	GB4462-5	Brownish-green consolidated clay	142	145	1.96	1.69
1	18-21	GB4462-5	Brownish-green consolidated clay	153	153	1.98	1.72
2	0-2	GB4462-6	Black mud with microbial mat filaments	9, 13	11	2.02	8.48
2	2-4	GB4462-6	Black mud with microbial mat filaments	-	22	1.97	8.65
2	4-6	GB4462-6	Brownish-green diatomaceous mud	20	20	1.95	2.51
2	6-8	GB4462-6	Brownish-green diatomaceous mud	-	47	1.95	3.38
2	8-10	GB4462-6	Brownish-green diatomaceous mud	-	60	1.95	1.48
2	10-12	GB4462-6	Brownish-green diatomaceous mud	69, 77	73	1.94	4.19
2	12-15	GB4462-6	Brownish-green diatomaceous mud	-	87	2.02	1.69
2	15-18	GB4462-6	Brownish-green diatomaceous mud	118	105	1.95	2.01
2	18-21	GB4462-6	Brownish-green diatomaceous mud	109	125	1.94	1.38
3	0-2	GB4462-3	Black mud with microbial mat filaments	3.2	3.2	1.96	7.31
3	2-4	GB4462-3	Brownish-green diatomaceous mud	-	8	1.96	3.91

3	4-6	GB4462-3	Brownish-green diatomaceous mud	15	15	2.00	2.86
3	6-8	GB4462-3	Brownish-green diatomaceous mud	-	26	2.02	5.00
3	8-10	GB4462-3	Brownish-green diatomaceous mud	34	34	1.97	2.02
3	10-12	GB4462-3	Brownish-green diatomaceous mud	-	43	2.01	1.86
3	12-15	GB4462-3	Brownish-green diatomaceous mud	-	54	1.94	1.78
3	15-18	GB4462-3	Brownish-green diatomaceous mud	61	66	2.01	1.43
3	18-21	GB4462-3	Brownish-green diatomaceous mud	83	80	1.96	1.98
4	0-2	GB4462-8	Black mud	0	0	1.93	3.44
4	2-4	GB4462-8	Brownish-green diatomaceous mud	1.5	8	2.01	3.17
4	4-6	GB4462-8	Brownish-green diatomaceous mud	16	16	1.95	4.00
4	6-8	GB4462-8	Brownish-green diatomaceous mud	-	18	2.02	4.19
4	8-10	GB4462-8	Brownish-green diatomaceous mud	-	21	2.02	4.76
4	10-12	GB4462-8	Brownish-green diatomaceous mud	-	23	1.95	4.84
4	12-15	GB4462-8	Brownish-green diatomaceous mud	-	25	1.95	5.74
4	15-18	GB4462-8	Sample lost during collection	-	-	-	-
4	18-21	GB4462-8	Sample lost during collection	29	-	-	-

Table 1. Sediment geochemical and lipid proxy data (continued).

Core ^a	Depth interval (cmbsf)	Alvin dive # and core ID	TEX ₈₆ Core GDGT ^c	TEX ₈₆ Core GDGT ^d	TEX ₈₆ Reconstructed SSTs (Kim et al., 2010) ^e	RI ^f	MI ^g	TEX ₈₆ 1G-GDGT ^c	TEX ₈₆ Core GDGT ^c
1	0-2	GB4462-5	0.56	-0.25	21.2	2.44	0.34	0.58	0.56
1	2-4	GB4462-5	0.58	-0.23	22.6	2.45	0.38	0.58	0.58
1	4-6	GB4462-5	0.58	-0.24	22.3	2.48	0.36	0.55	0.58
1	6-8	GB4462-5	0.58	-0.24	22.2	2.55	0.35	0.57	0.58
1	8-10	GB4462-5	0.59	-0.23	22.9	2.60	0.34	0.72	0.59
1	10-12	GB4462-5	0.57	-0.25	21.8	2.63	0.31	0.70	0.57
1	12-15	GB4462-5	0.61	-0.22	23.8	2.65	0.37	0.69	0.61
1	15-18	GB4462-5	0.61	-0.22	23.9	2.66	0.36	-	0.61
1	18-21	GB4462-5	0.63	-0.20	24.9	2.66	0.38	-	0.63
2	0-2	GB4462-6	0.55	-0.26	20.6	2.52	0.32	0.46	0.55
2	2-4	GB4462-6	0.54	-0.27	20.4	2.52	0.32	0.58	0.54
2	4-6	GB4462-6	0.54	-0.27	20.4	2.53	0.33	0.60	0.54
2	6-8	GB4462-6	0.56	-0.25	21.5	2.68	0.29	0.71	0.56
2	8-10	GB4462-6	0.58	-0.25	21.7	2.70	0.29	0.70	0.58
2	10-12	GB4462-6	0.57	-0.24	21.9	2.71	0.28	0.68	0.57
2	12-15	GB4462-6	0.57	-0.24	21.9	2.73	0.28	0.73	0.57
2	15-18	GB4462-6	0.58	-0.23	22.6	2.68	0.31	-	0.58
2	18-21	GB4462-6	0.59	-0.23	22.8	2.74	0.28	-	0.59
3	0-2	GB4462-3	0.54	-0.27	20.2	2.41	0.37	0.53	0.54
3	2-4	GB4462-3	0.53	-0.27	19.8	2.62	0.27	0.49	0.53
3	4-6	GB4462-3	0.53	-0.27	19.9	2.53	0.31	0.56	0.53
3	6-8	GB4462-3	0.54	-0.27	20.3	2.50	0.33	0.54	0.54

3	8-10	GB4462-3	0.53	-0.27	19.9	2.54	0.31	0.61	0.53
3	10-12	GB4462-3	0.54	-0.27	20.3	2.64	0.27	0.74	0.54
3	12-15	GB4462-3	0.56	-0.25	21.5	2.56	0.30	0.69	0.56
3	15-18	GB4462-3	0.55	-0.26	20.9	2.77	0.26	0.74	0.55
3	18-21	GB4462-3	0.57	-0.25	21.6	2.68	0.29	0.66	0.57
4	0-2	GB4462-8	0.54	-0.27	20.4	2.43	0.35	0.54	0.54
4	2-4	GB4462-8	0.53	-0.27	20.0	2.59	0.30	0.37	0.53
4	4-6	GB4462-8	0.54	-0.27	20.2	2.55	0.31	0.43	0.54
4	6-8	GB4462-8	0.52	-0.28	19.3	2.55	0.29	0.45	0.52
4	8-10	GB4462-8	0.53	-0.27	19.9	2.69	0.26	-	0.53
4	10-12	GB4462-8	0.53	-0.27	19.8	2.54	0.30	-	0.53
4	12-15	GB4462-8	0.53	-0.28	19.7	2.90	0.20	-	0.53
4	15-18	GB4462-8	-	-	-	-	-	-	-
4	18-21	GB4462-8	-	-	-	-	-	-	-

^a Collected core numbers are relabelled in the sample name to reflect a relative transect position (1-4).

^b Sediment lithology based on freeze-dried sediments.

^c $TEX_{86} = (GDGT-2 + GDGT-3 + GDGT-5)/(GDGT-1 + GDGT-2 + GDGT-3 + GDGT-5)$, (Schouten et al., 2002) applied to both core GDGTs and 1-glycosyl-GDGTs. (1)

^d $TEX_{86}^H = \log ((GDGT-2 + GDGT-3 + GDGT-5)/(GDGT-1 + GDGT-2 + GDGT-3 + GDGT-5))$, for sediments outside the polar regions (Kim et al., 2010).

^e Following the mean annual sea surface calibration of 0 m water depth ($SST = 68.4 \times TEX_{86}^H + 38.6$) of Kim et al. (2010).

^f Ring index (RI) = $0 \times (GDGT-0) + 1 \times (GDGT-1) + 2 \times (GDGT-2) + 3 \times (GDGT-3) + 4 \times (GDGT-4) + 5 \times (GDGT-5) / \Sigma GDGTs$, adapted from Pearson et al. (2004) and promoted by Zeng et al. (2016). (2)

^g Methane index (MI) = $(GDGT-1 + GDGT-2 + GDGT-3)/(GDGT-1 + GDGT-2 + GDGT-3 + GDGT-5 + GDGT-5')$ by Zhang et al. (2011).

2.2. Lipid extraction

Lipid extractions followed a modified Bligh and Dyer protocol laid out in Bentley et al. (2022) and following Sturt et al., 2004. A subsample of freeze-dried sediment was added to a Teflon[®] centrifuge tube followed by the addition of 6 ml of mix A solvent solution comprising of 2:1:0.8 v/v/v methanol (MeOH), dichloromethane (DCM), and phosphate buffer (5.5 g L⁻¹ Na₂HPO₄; Avantor Performance Materials, LLC, adjusted to pH of 7.4 with HCl; Anachemia Co.). The solvent sediment mixture was further spiked Samples were spiked with a recovery standard (1-alkyl-2-acetoxy-3-sn-glycero-3-phosphocholine (PAF); recovery standard purchased from Avanti Polar Lipids, Inc.) The sediment/solutionslurry was sonicated for 5 min before being then centrifuged for 5 min at 1250 rpm. The resulting supernatant was added to a separatory funnel. This procedure was performed twice and then followed before being joined by two- replicate extractions using mix B, a 2:1:0.8; v/v/v solution of MeOH, DCM, and trichloroacetic acid buffer (50 g/L C₂HCl₃O₂; Avantor Performance Materials, LLC, of pH 2) and a final two replicate extractions using mix C, a 5:1 v/v solution of MeOH and DCM. Once complete, the combined A, B, and C mixed extracts were then back extracted in the and extracted using a modified Bligh and Dyer protocol after Sturt et al. (2004). The extraction involved six steps using 3 different solvent mixtures consisted of a 6 ml of solvent separatory funnel by washing the organic phase with 1:1 v/v milliQ water and DCM, followed by 6 additional washes (×3 with DCM followed by ×3 milliQ water washes). For each step, the organic fraction was collected in a beaker and evaporated to dryness at 60 °C under a gentle steam of dry nitrogen, mixture, sonicated for 5 min, and centrifuged for 5 min, at 1250 rpm. After each extraction step, the solvent was decanted and combined in a separation funnel. The combined extract was purified with milliQ water, heated at ca. 60 °C, and evaporated to dryness under a gentle steam of dry nitrogen. The first four steps involved solvent mixtures of methanol/dichloromethane/buffer [2:1:0.8; v/v/v]. From this, the first two steps used a phosphate buffer (5.5 g/L Na₂HPO₄; Avantor Performance Materials, LLC.) adjusted to pH of 7.4 with HCl; Anachemia Co.), while

Formatted: Superscript

Formatted: Superscript

Formatted: Not Highlight

Formatted: Not Highlight

Formatted: Not Highlight

the third and fourth steps employed a trichloroacetic acid buffer (50 g/L C₂HCl₃O₂; Avantor Performance Materials, LLC; (pH of 2). The final two steps used a solvent mixture of methanol/dichloromethane [5:1; v/v]. Each extraction step consisted of a 6 ml of solvent mixture, sonicated for 5 min, and centrifuged for 5 min at 1250 rpm. After each extraction step, the solvent was decanted and combined in a separation funnel. The combined extract was purified with milliQ water, heated at ca. 60 °C, and evaporated to dryness under a gentle stream of dry nitrogen. The resulting total lipid extract (TLE) was transferred to preweighed autosampler vials using DCM:MeOH 9:9 v/v, was then spiked with -1, 2-dihencicosanoyl-*sn*-glycero-3-phosphocholine (C₂₁-PC; Avanti Polar Lipids, Inc.) and subsequently stored at -20 °C before it was injected for mass spectral analysis.

2.3. High performance liquid chromatography – mass spectrometry (HPLC-MS)

A Mass spectrometric analyses were performed on an Agilent Technologies 1260 Infinity II HPLC coupled to an Agilent Technologies 6530 quadrupole time-of-flight mass spectrometer (qToF-MS) operated in positive mode. Chromatographic separation used a reverse phase method outlined by Zhu et al. (2013). The HPLC was fitted with using an Agilent Technologies ZORBAX RRHD Eclipse Plus C₁₈ (2.1 mm × 150 mm × 1.8 μm) reverse phase column, fitted with a guard column and maintained at 45 °C. Samples were pre-concentrated and injection solvent was methanol. An aliquot of each sample representing 1% of the TLE was then analyzed. The flow rate was set to 0.25 mL min⁻¹, and flow rate was established with the gradients were: mobile phase A (consisting of methanol/formic acid/ammonium hydroxide [100:0.04:0.10] v/v/v) held at 100% for 10 min., thereafter mixed following a linear gradient with mobile phase B (propan-2-ol/formic acid/ammonium hydroxide (100:0.04:0.10 v/v/v) to followed by a linear gradient to 24%, 65%, and 70% mixing with over mobile phase B (propan-2-ol/formic acid/ammonium hydroxide [100:0.04:0.10] v/v/v) extending for 5, 75, and 15 min., intervals, respectively. a linear gradient to 65% B for 75 min., followed by 70% B for 15 min., that finished by re-equilibrating the system with 100% mobile phase A for 15 min. The injection solvent was methanol. The effluent was ionized by an reverse phase electrospray ionization method source with a gas temperature of 300 °C, a 3 L min⁻¹ drying gas flow and a 5.33 μA source current. The mass spectrometer was set to a 100–3000 *m/z* with a scan range from 100–3000 *m/z* was chosen for its ability to simultaneous resolve both archaeal IPLs and CLs. [More about the ms method.](#) An aliquot of each sample representing 1% of the TLE was analyzed using an Agilent Technologies 1260 Infinity II HPLC coupled to an Agilent Technologies 6530 quadrupole time-of-flight mass spectrometer (qToF-MS). Separation was achieved following the method described by Zhu et al. (2013) using an Agilent Technologies ZORBAX RRHD Eclipse Plus C₁₈ (2.1 mm × 150 mm × 1.8 μm) reverse phase column, fitted with a guard column and maintained at 45 °C. The flow rate was set to 0.25 mL/min. and the gradients were: mobile phase A (methanol/formic acid/ammonium hydroxide [100:0.04:0.10] v/v/v) held at 100% for 10 min., followed by a linear gradient to 24% mixing with mobile phase B (propan-2-ol/formic acid/ammonium hydroxide [100:0.04:0.10] v/v/v) extending for 5 min., a linear gradient to 65% B for 75 min., followed by 70% B for 15 min., that finished by re-equilibrating with 100% A for 15 min. The injection solvent was methanol.

Analyte identification was achieved by accurate mass resolution, mass spectral analysis using Agilent Technology's MassHunter software and by comparison of fragmentation patterns with the literature (e.g., Knappy et al., 2009; Liu et al., 2010; Yoshinaga et al., 2011 – see Bentley et al., 2022 for further details). Mass fragments consistent with the loss of a biphytane (*m/z* 743.7) were screened for all archaeal lipids. Quantification was achieved by summing the integration of peak areas of adducts [M+H]⁺, [M+NH₄]⁺, and [M+Na]⁺ adducts for the respective GDGTs IPLs and CLs of interest. The signals for these compounds were monitored as [M+H]⁺ on the *m/z* 1464.38, 1462.36, 1460.34, 1458.33, 1456.31, 1454.30 mass chromatograms. Additionally, mass fragments consistent with the loss of a biphytane (*m/z* 743.7) were observed. Once the integrated peak areas were determined for each GDGT, concentration values were obtained relative to the internal C₂₁-PC standard and reported in μg/g dry sediment weight.

Response factors were also determined by a series of injections of a standard solution containing: *sn*-PAF, C₂₁-PC, 1,2-diacyl-3-O-(α-D-galactosyl-1-6)-β-D-galactosyl-*sn*-glycerol (DGDG), 1,2-diacyl-3-O-β-D-galactosyl-*sn*-glycerol (MGDG), 1-alkyl-2-acetyl-*sn*-glycero-3-phosphocholine (PAF), 1,2-di-O-phytanil-*sn*-glycerol (Archaeol), 1',3'-bis[1,2-dimyrystoyl-*sn*-glycero-3-phospho]-glycerol (14:0 Cardiolipin), 1,2-

Formatted: Superscript

Formatted: Superscript

Formatted: Font: Not Italic, Font color: Auto

diheneicosanoyl-*sn*-glycero-3-phosphocholine (C₂₄-PC) from Avanti Polar Lipids, Inc., USA, and 2,2'-di-O-decyl-3,3'-di-O-(1'',ω''-eicosanyl)-1,1'-di-(rac-glycerol) (C₄₆-GTGT) from Pandion Laboratories, LLC in amounts ranging from 100 pg to 30 ng. Concentrations of the standard mix were then calculated from peak areas of molecular ions in mass chromatograms. Response factors were calculated relative to the C₂₁-PC, and the appropriate correction factor was then applied to the particular lipid class of interest.

A series of samples were re-run to identify or confirm deviations in the data set. The variations between the concentrations of GDGTs in the re-run and the initial runs yielded a maximum difference of $\sim \pm 4 \mu\text{g}\cdot\text{g}^{-1}$ per GDGT compound, providing confidence in the initial results and confirming the presence of two outliers in the data set (Bentley et al., 2022). These outliers are Core 4 at 8–10 cm, with abnormally low concentrations of all compounds that is likely ion suppression from a sample heavily impregnated with oil, and Core 3 at 15–18 cm, which contains relatively high lipid concentrations that are yet to be explained.

3. Results and Discussion

3.1. Archaeal lipid diversity and heterotrophic loss

The Cathedral Hill transect sediments have *i*GDGTs containing 0–4 cyclopentyl (GDGT 0–4) as well as crenarchaeol (Cren) and the isomer of crenarchaeol (Cren') that contains five rings (four cyclopentyl and one cyclohexyl moiety) (Table S1). Branched GDGTs include 1a-c, 2a-c, and 3a were found to have discontinuous and/or low absolute abundances, with some compound classes not being detected (i.e. *br*GDGT-3b). The *br*GDGTs are therefore not further examined in this study. For cores 1 to 3 the concentrations of all *i*GDGT compounds systematically decrease with depth (Figure 2). Bentley et al. (2021,2022) established the sedimentation of archaeal lipids from the upper water column as being uniform both in terms of spatial loading across the length of the transect as well as over the past 52.5–105 yrs. of sedimentation as penetrated by the length of the push core. From this, it is estimated that $\sim 70.57 \pm 23.5 \mu\text{g } i\text{GDGTs}\cdot\text{g}^{-1}\cdot\text{yr}^{-1}$ is being deposited on the seafloor from the upper overlying water column. However, for cores closest to the vent site, lipid abundances exhibited a much sharper decrease with depth, which Bentley et al. (2021,2022) attribute to the turnover of archaeal lipids coupled to, but not directly caused by, hydrothermalism. For cores 1 and 2, losses reach as high as 94% within the upper 21 cmbsf (cm below sea floor). The lipid loss is less severe for core 3 at $\sim 60\%$. For the ambient core 4, *i*GDGTs have similar down core stratigraphic trends with a near-consistent average of 400 $\mu\text{g/g}$ sediment concentration and no systematic loss of lipids.

Due to the extreme vent fluid conditions at Cathedral Hill, the identified archaeal *i*GDGT-based IPLs within the sediments most likely represent the composition of cellular membrane material from active-archaeal communities residing-living in the sediments. These lipids have exclusively monoglycosyl (1G) or diglycosyl (2G) head groups linked to a 2,3-*sn*-glycerol. Within the pyrolytic environment the transformation of IPL *i*GDGTs could hypothetically add to the core *i*GDGT lipid pool. Similar to CLs, the 1G-GDGTs range from -0 to -4 and include Cren and Cren'. Surface concentrations of these lipids are $\sim 15 \mu\text{g}\cdot\text{g}^{-1}\cdot\text{sed}^{-1}$ in cores 1 to 3 (residing within the microbial mat) and $11 \mu\text{g}\cdot\text{g}^{-1}\cdot\text{sed}^{-1}$ for core 4 (Table S2). Also similar to the CLs, the archaeal IPL concentrations decrease down core and are tightly controlled by porewater temperatures (Table S2). For cores 1 and 2 the maximum depths for detectable 1G-GDGTs are 15–18 and 12–15 cmbsf, corresponding to vent porewater temperatures of 145 and 87 °C, respectively. In core 3, 1G-GDGTs persists down core with a consistent lipid depletion that reaches its lowest concentration of $5.22 \mu\text{g}\cdot\text{g}^{-1}\cdot\text{sed}^{-1}$ in the bottom of the core at 18–21 cmbsf sediment depth where porewater temperatures rise to 80 °C. In core 4, which is most similar to the ambient ocean bottom conditions and falls outside of the area covered by the microbial mat, the lipid concentrations average is $\sim 8 \mu\text{g}\cdot\text{g}^{-1}$ across the depth of the core. The 2G-GDGTs have 0 to 2 cyclopentyl rings that for cores 1 and 2 are restricted to the upper 4 to 6 cmbsf. These lipids are not further investigated in this study as 2G-GDGTs are of limited abundance (max summed concentrations $< 7 \mu\text{g}\cdot\text{g}^{-1}\cdot\text{sed}^{-1}$) and their structural diversities negligibly effect isoprenoid-based proxies.

Lipid-based proxies for the calibration or reconstruction of paleoclimate records such as TEX₈₆, BIT, CBT, and MBT, are based on environmentally scaled loadings of select GDGT compound classes. These proxies could be negatively impacted should other ocean floor sediment systems experience high rates of lipid turnover (Lengger et al., 2014). To evaluate whether down-core depletions of lipid concentrations impacted

Formatted: Superscript

Formatted: Superscript

Formatted: Superscript

Formatted: Superscript

tetraether-based proxies, the concentrations of the highly abundant GDGT-0 was plotted relative to the TEX₈₆ ratio lipids (*i*GDGT-1, -2, -3, and Cren') (Figure 3A). For figure 3A, straight lines in the logarithmic plot indicate near-equal depletion rates between the paired x- and y-axis lipid classes. Similarly, parallel lines betweenfor the various lipid pairs also indicatess near-equal depletion rates, with vertical offsets between pairs marking different initial starting abundances between the paired-of the lipid classes. In this regard, *i*GDGT-0, -1, -2, and Cren' have undergone the same rate of turnover. However, the depletion rate of *i*GDGT-3's is lower than that of other lipid classes for cores 1 and 2. Although, this may represent a distinct resilience to turnover, we suggest it instead results from overprinting by the subsurface hyperthermophilic archaeal community (see below).

To better track changes across each core, the degradation rate constants (*k'*) of TEX₈₆ lipid classes were calculated for each push core (Figure A2; Table A3) using a first-order kinetic model:

$$C_t = C_i \cdot e^{-k't} \quad (5)$$

in which *C_t* and *C_i* are concentration at time (*t*) and the initial concentration, respectively (Schouten et al., 2010). Rearranging Eq. 5, the *k'* were calculated as

$$k' = (-\ln[C_t / C_i]) / t \quad (6)$$

From these data, it is evident that the down core concentrations of each lipid decrease_s at equivalent rates for all but core 2 (i.e. they have the same slopes for their rates of decay; *m*_{log *k'*}). This is consistent with the TEX₈₆ *i*GDGT lipid classes largely being removed from the sediment lipid pool in a non-selective manner.

~~Lastly, Based on these results, the~~ TEX₈₆, RI, and MI values were plotted against their respective summed *i*GDGTs lipid concentrations (Fig 3B–D). For samples located within the habitable zone (having porewaters ranging from 0–123 °C; Kashefi and Lovley, 2003), no correlation is observed between the lipid abundances and proxy ratios of TEX₈₆, RI, or MI (Figure 3B–D). This further suggests these proxies are not affected by turnover in the habitable zone. However, once sediment burial reaches beyond the habitable zone, TEX₈₆ ratios trend to higher values (similarly also reflected in GDGT-3 concentration trends of Figure 3A). Collectively, these data strongly indicate that archaeal lipid turnover is largely nonselective of the TEX₈₆ lipid classes and will therefore theoretically not in and of itself-themselves significantly impact archaeal lipid paleoclimate proxy reconstructions.

Apart from paleoclimate reconstructions, ~~the~~ archaeal lipid ~~data-CLs are can also sometimes be used to used~~ to resolve ~~some aspects of aspects of the~~ localized biogeochemical cycles, ~~within sediments present at the vent site.~~ To this end, the location and degree of anaerobic oxidation of methane (AOM) is determined by methane and archaeal lipid isotope measures (e.g. Boetius et al., 2000; Schouten et al., 2003; Stadnitskaia et al., 2008; Biddle et al., 2012) as well as by the proportional abundances of cGDGTs in the form of the methane index (MI; Zhang et al., 2011; Carr et al., 2018; Petrick et al., 2019). With respect to the latter, the MI proxy is used to differentiate regions of normal marine (with values between 0–0.3) and active AOM conditions in an around cold seeps (where values >0.5–1 are reported for gas hydrate impacted sediments and subsurface environments with high AOM levels). To our knowledge, the use this proxy for hydrothermal vent systems has not been thoroughly investigated even though this microbial process Maximal anaerobic oxidation of methane (AOM) at Guaymas Basin has been well observeddocumented at Guaymas Basin. at 35 to 90 °C. For example, highly ¹³C-depleted CLs reaching up to -70‰ in hydrothermal vent sediments with porewater temperatures as high as 95 °C indicates thermophilic archaea actively engaging in AOM (Schouten et al., 2003). Biddle et al. (2012) through the detection of relevant archaeal communities by 16S RNA in conjunction with highly depleted methane carbon isotope values determined active AOM spanning 35 to 90 °C pore water conditions. ~~but~~ AOM is not likely to be the dominant form of carbon and sulfur metabolism as it generally accounts for less than 5% of sulfate reduction (Kallmeyer and Boetius, 2004). For example, highly ¹³C-depleted CLs reaching up -70‰ in hydrothermal vent sediments with porewater temperatures as high as 95 °C indicates thermophilic archaea actively engaging in AOM (Schouten et al., 2003). The methane index (MI; Table 1) can be used to differentiate regions of normal marine (values between 0–0.3) and active AOM conditions where values >0.5–1 for gas hydrate impacted sediments and subsurface environments with high levels of AOM (Stadnitskaia et al., 2008; Zhang et al., 2011). When applying the MI to the Cathedral Hill sediments push core transect survey very low values (ranging from 0.2–0.38; Table 1) are recorded with no

Formatted: Space Before: 0 pt

Formatted: Space After: 0 pt

Formatted: Space Before: 0 pt

Formatted: Space Before: 0 pt

Formatted: Not Highlight

Formatted: Not Highlight

Formatted: Not Highlight

Formatted: Not Highlight

Formatted: Not Highlight

Formatted: Not Highlight

Formatted: Not Highlight

Formatted: Not Highlight

Formatted: Not Highlight

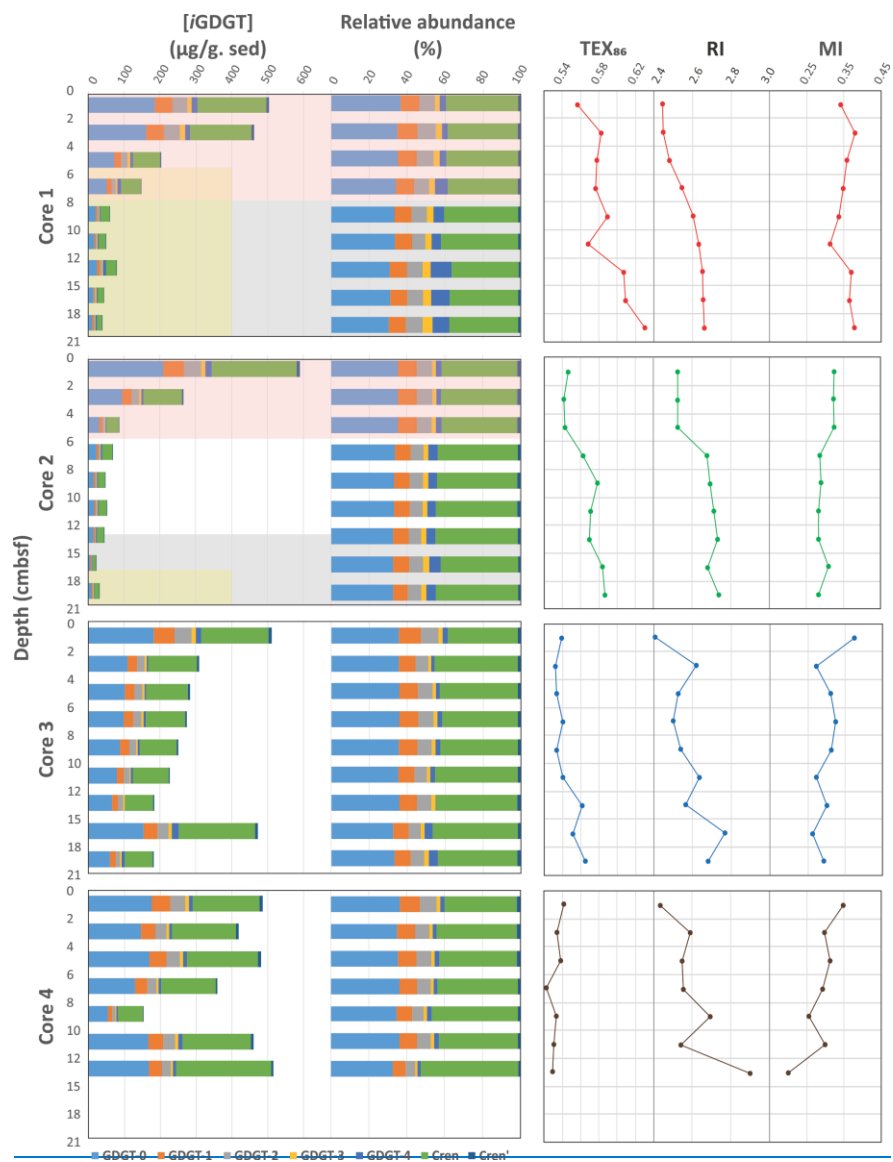
Formatted: Not Highlight

Formatted: Not Highlight

Formatted: Not Highlight

correspondence to thermal controls [across the vent transect](#). Although, it could be considered that this arises from [a lack of AOM within these sediments](#) the low MI values are consistent with [a high upper water column iGDGTs loading as estimated by Bentley et al. \(2022\)](#). ~~selective degradation; the very low MI values are equally explained by broad loading of iGDGTs from the upper water column. As such, the low AOM activities may also indicate microbial ammonia oxidation, which has been shown to influence the TEX₈₆ proxy (Hurley et al., 20016) is likely not a significant factor in this setting.~~ ▲

Formatted: Font color: Auto



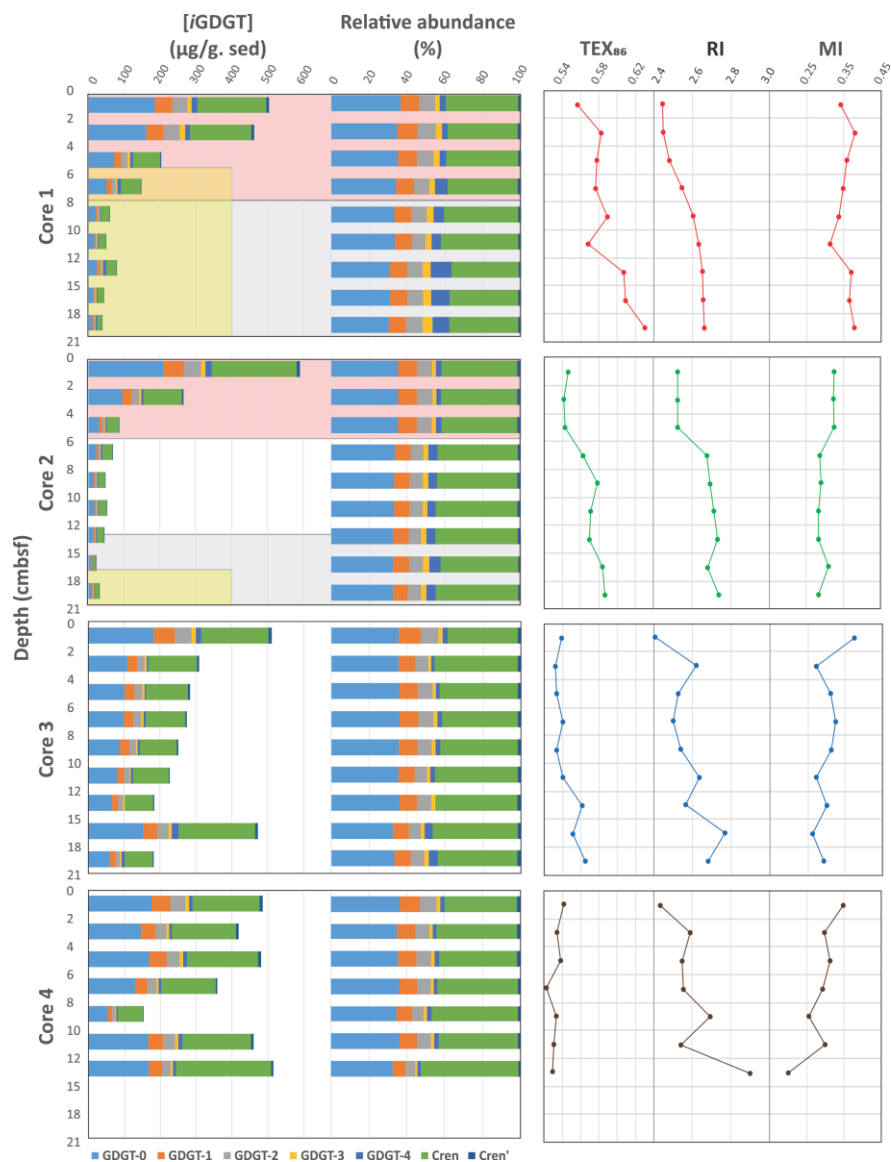
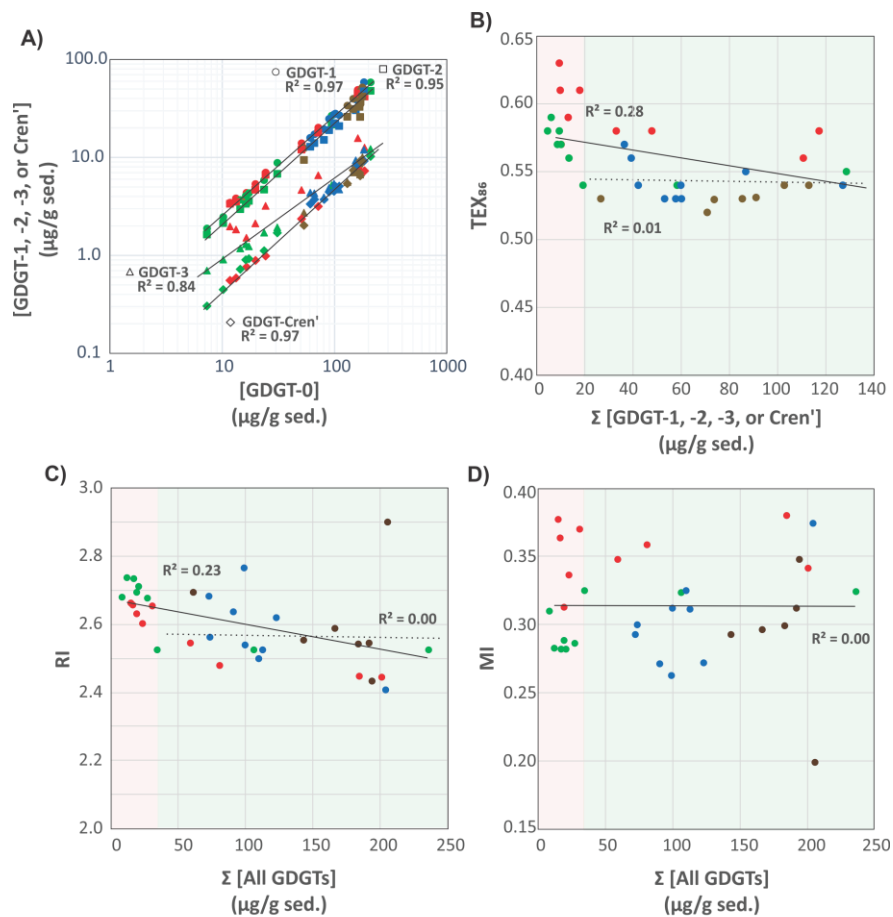


FIGURE 2. Down core profiles of the Cathedral Hill core *i*GDGTs absolute and relative lipid abundances and their generated *i*GDGT proxies: TEX₈₆, RI, and MI. Pink regions indicate transect intervals within zones of active GDGT lipid heterotrophy (Bentley et al., 2021). Grey regions mark regions where porewater temperatures exceed 123 °C marking a zone beyond the upper thermal limit of life. Yellow fields indicate regions where oil generation and hydrocarbon degradation has been noted to occur (Dalzell et al., 2021).

498
499



• Core 1 • Core 2 • Core 3 • Core 4

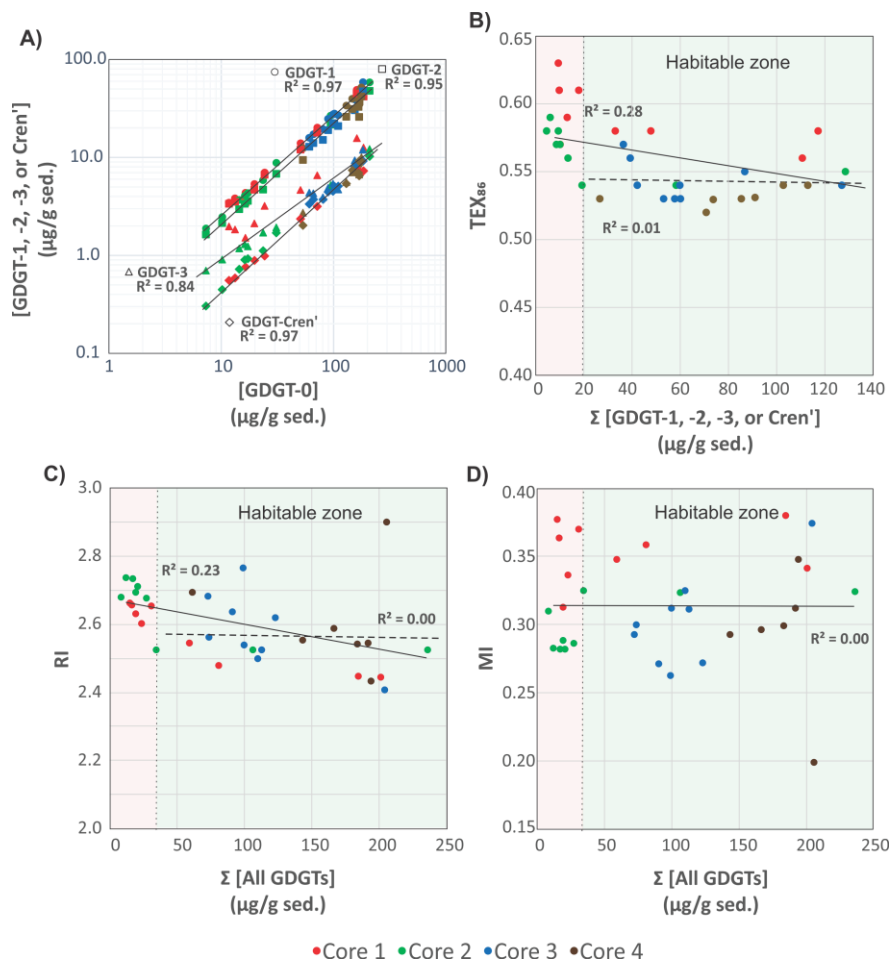


FIGURE 3. A) Comparison of TEX₈₆ lipid concentrations GDGT-1 (circles), -2 (squares), -3 (triangles), and Cren' (diamonds) relative to the GDGT-0. Comparison of B) TEX₈₆, C) RI, and D) MI proxy values relative to summed *i*GDGTs abundances of the Cathedral Hill transect cores. Light green and pink regions indicate areas within and outside the habitable zone of life. Solid and dotted regression lines mark the total number of samples investigated for this study ($n=34$) and those that only reside within the habitable zone where up to 94% of the archaeal lipid turnover occurs ($n=22$), respectively.

3.2. TEX₈₆ and reconstructed SSTs

McClymont et al. (2012) reported a GDGT-based reconstructed annual SSTs of 16–18 °C for ambient sediment in the Guaymas Basin during an annual cycle from 1996–1997 following the calibration model for sediments outside of polar regions proposed by Kim et al. (2010). These authors demonstrated the temperatures derived from the TEX₈₆ reconstruction were significantly lower than those ~~derived-produced by~~ ~~from~~ the closely co-varying U₃₇^{K'}, an alkenone lipid-based paleoclimate proxy (Brassell et al., 1986), and satellite measured estimates that jointly ~~produced-estimated~~ a mean annual sea surface temperature (MASST) of 23 °C. The longer 21-year (1982–2004) satellite-derived MASST is also reported to be higher at 24 °C (Herrera-Cervantes et al., 2007). Although the sites and time frames of these surveys do not match that of the Cathedral Hill survey, they do provide context to what our reconstructed TEX₈₆ values should record.

The high sedimentation rate at Cathedral Hill has resulted in near homogenous inputs of organic matter from the upper water column across the transect area (Dalzell et al., 2021; Bentley et al., 2021,2022). Therefore, TEX₈₆ reconstructions should produce equivalent cross-transect trends with sediment depth. Nonetheless, as with changes in the archaeal lipid concentrations, the profiles of *i*GDGT proxies TEX₈₆ and RI of the transect similarly have down core trends (Figure 2; Bentley et al., 2021,2022). For core 4, TEX₈₆ span a narrow range of values (n=7; 0.52–0.54, avg. 0.53 ± 0.01; Figure 4A) across a period of ~ 37.5 to 75 yrs. To a slightly lesser degree, the shallow-surface samples (0–2 cmbsf) across the transect also display near-equal values to core 4 (n=4; 0.56–0.54; avg. 0.55 ± 0.01). These values mark a TEX₈₆^H reconstructed mean annual SST of 19.3–20.4 °C following the Kim et al. (2010) calibration model (Table 1). However, the TEX₈₆ values recorded in cores 1 to 3 at Cathedral Hill have considerably larger ranges that systematically increase with rising porewater temperatures (R² = 0.83; Table 1; Figure 2 and 4A). This increase is most noticeable in core 1 where the highest TEX₈₆ values are obtained from the bottom core sediments (10–21 cmbsf) where TEX₈₆ values span 0.57–0.63 (Table 1; Fig 4A) corresponding to a TEX₈₆^H reconstructed SST change of 3.1 °C marking a range from 21.8 to 24.9 °C (Table 1). Since the Cathedral Hill transect only spans ~8 m, the fundamental driver for the proxy's increases must be exposure to *in situ* vent fluid temperatures (Figure 4).

Two mechanisms are considered for the observed proxy variations. The first is that progressive ring-loss due to carbon-carbon bond cleavage of pentacyclic rings moieties by exposure to the sharp geothermal gradient ~~at Cathedral Hill~~ acts to systematically attenuate the *i*GDGT lipid pool. Hydrous pyrolysis experiments conducted by Schouten et al. (2004) demonstrated that at extreme temperatures (ca. >160 °C), TEX₈₆ values become negatively impacted by the preferential destruction of polycyclic GDGTs. Such losses produce progressively lower ratio values. Although, the transect sediment porewaters do not reach the pyrolytic temperatures of the Schouten et al. (2004) experiment, they are high enough to generate hydrocarbons (Dalzell et al., 2021) and thermochemically degrade *i*GDGTs in the hottest regions of the transect. However, the observed stratigraphic TEX₈₆ trends do not match those of predicted ring loss as the values increase rather than decrease in relation to elevated porewater condition. Nonetheless, the thermochemical oxidative loss of GDGTs and its effect on the TEX₈₆ ratio is further explored below (section 3.4).

The second mechanism is that subsurface microbial communities donate enough core GDGTs to overprint the detrital signal source. The RI (Figure 4B) values were similarly compared to recorded porewater temperatures to better interpret the TEX₈₆ trends and to ensure that the Cathedral Hill reconstructed temperatures are influenced by the subsurface microbial community. In this regard, RI is used to monitor the adaptive response of an archaeal community at the hydrothermal vent site. Lipid cyclization is an adaptive response to changing environmental temperature or acidity in which an archaeon increases its rigidity by decreasing the fluidity and permeability of its cellular membrane that, therefore, also further regulates the flow of solutes and nutrients in and out of the cell (Gliozzi et al., 1983; De Rosa and Gambacorta, 1988; Uda et al., 2001; Schouten et al., 2002; Macalady et al., 2004; Boyd et al., 2013). Both cores 1 and 2 have RI values highly correlated to temperature (R² = 0.87 and 0.75, respectively) consistent with heat stress adaption. As such, a significant proportion of the measured *i*GDGTs likely emanate from archaeal communities living in the shallow sediments of Cathedral Hill. ~~In this regard~~ ~~As such~~, the lipid cyclization pattern may reflect stratigraphically discrete thermophilic to hyperthermophilic communities that are selectively adapted to more extreme temperature conditions.

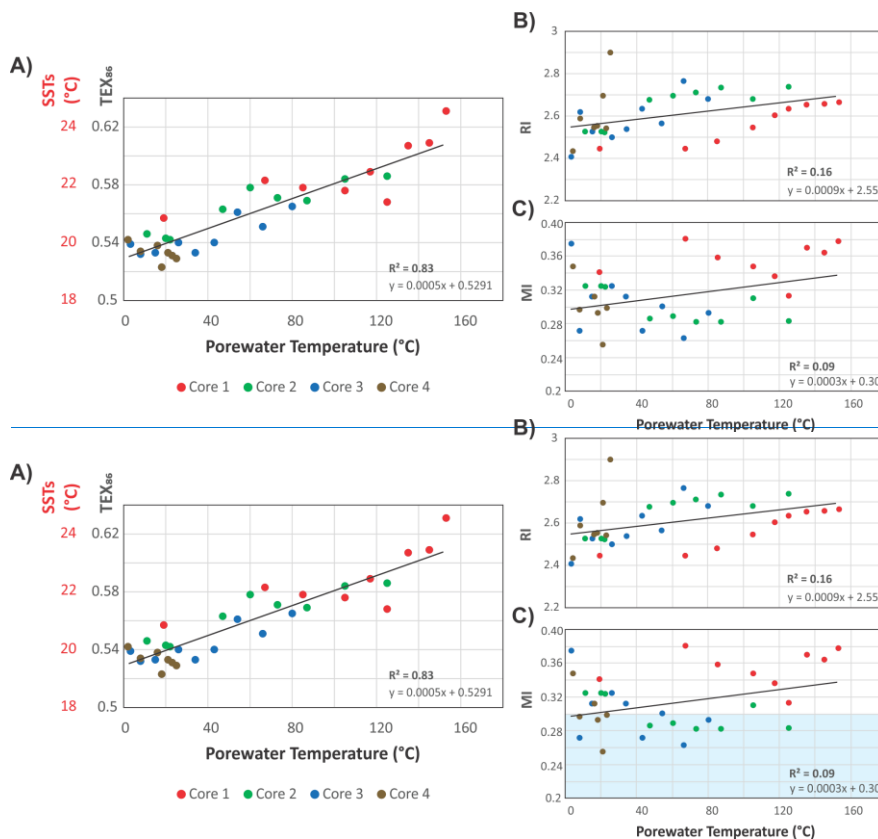


FIGURE 4. Cross plots of A) TEX₈₆, B) RI, and C) MI, *i*GDGT proxies versus porewater temperature. TEX₈₆^H reconstructed MASSTs are based on Kim et al. (2010). [Blue field indicates MI values for normal marine conditions \(Zang et al., 2011\).](#)

3.3. Lipid signal sourcing

To evaluate the sources of measured archaeal lipids, *core-CL* and *IPL*TEX₈₆ indices were compared as signal response loadings from their respective pools of living and dead cellular debris (Figure 5). For cores 1, 2, and 3 the 1G-*i*GDGT *IPL*TEX₈₆ measures are *positively* correlated with temperature ($R^2 = 0.46, 0.74$, and 0.66 , respectively; Figure 5A). In this regard, 1G-*i*GDGT *IPL*TEX₈₆ ratio appears to also measure *in situ* porewater temperatures. Factors such as community composition and adaptation may further impact the *IPL*TEX₈₆ ratio as the rates of changes between cores 1–3 are not the same. Similar to the *CL*-TEX₈₆ values, the *IPL*TEX₈₆ are not correlated to their summed TEX₈₆ lipid abundances (Figure 5B). Such a condition is consistent with the living lipid pool being modified by the archaeal community's response to thermal stress and not by subsequent thermal oxidative transformation occurring shortly after cell death.

Formatted: Subscript

The IPL and CL lipids of transect samples can be further grouped into three clusters (A, B, C), suggesting a mixed signal for the sourcing of archaeal GDGTs from both the living and dead pools of archaea (Figure 5C). In this plot, we assume that clusters falling on the 1:1 line indicate the living biota can equally contribute to the dead pool of total recovered GDGTs. Those off-axis contribute either less or more to one or the other lipid pool. The three clusters mark unique thermal zones within the transect area with cluster A being composed of the ambient core 2 to 4 seafloor surface samples; cluster B marking a mix of intermediate temperature samples from all cores; and cluster C being composed of high temperatures samples. The lipid groups likely mark distinct archaeal communities. As cluster B resides on the 1:1 line, the TEX₈₆ core lipids likely have a mixed of detrital and *in situ* inputs. Cluster C, however, appears likely dominated by *in situ* lipid production. The hyperthermophilic *Methanopyrus kandleri*, recovered from other Guaymas Basin sites (Teske et al., 2014), may represent one such archaeon contributing to the cluster C lipid pool. The thermal zonation and equivalent directionality of the resulting ratios (i.e. both CL and IPL-TEX₈₆ ratios increase with porewater temperature) further supports overprinting of the original CL-TEX₈₆ sea surface signal by the ocean bottom sediment archaeal community as a mechanism for the observed CL-TEX₈₆ trends.

Collectively, these results suggest the source of the archaeal core lipids measured in the TEX₈₆ and RI indices progressively become more dominated by subsurface microbial communities adapted to the hotter hydrothermal vent fluids. Our results also indicate that in select natural environments, such as hydrothermal vent complexes, the TEX₈₆ SST-proxy may entirely record ocean bottom sediment porewater temperatures. To our knowledge, a clear case of overprinting to this level has not yet been demonstrated.

Formatted: Subscript

Formatted: Subscript

Formatted: Subscript

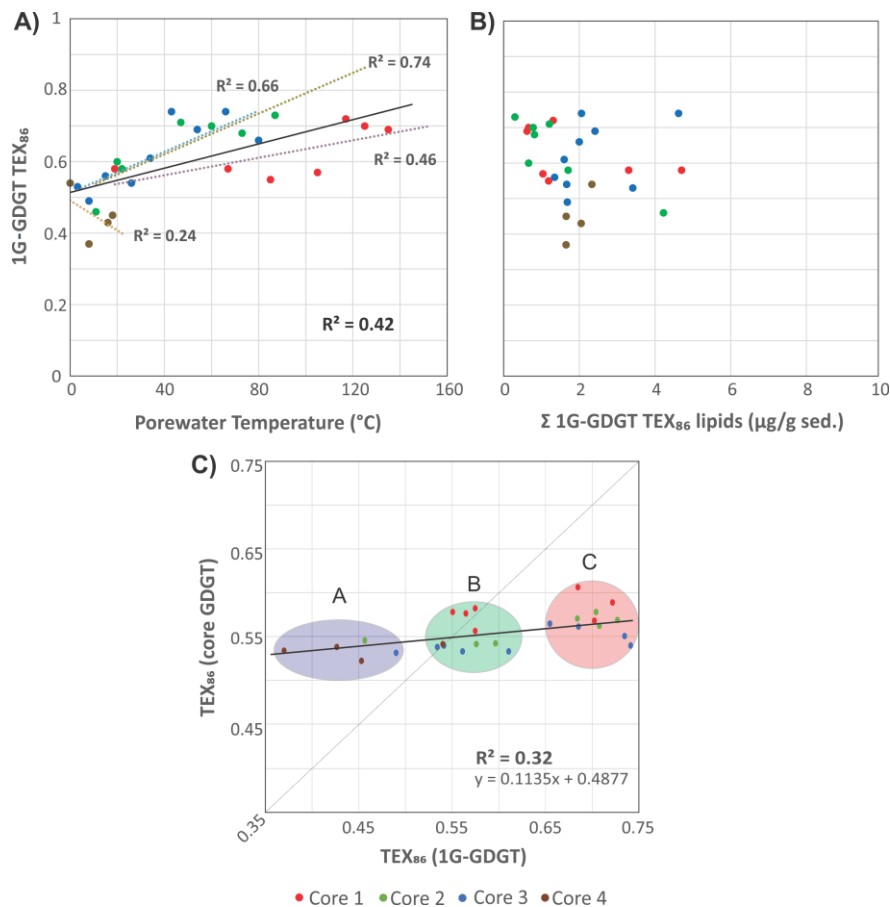


FIGURE 5. Cross plots of 1G-iGDGTs $_{IPL}TEX_{86}$ versus (A) porewater temperatures and (B) the concentration of 1G-iGDGTs in the sediments. (C) TEX_{86} proxy of core GDGTs vs 1G-GDGTs. Clusters A–C may represent different archaeal communities that are providing varying inputs of iGDGT to the core GDGT lipid pool. The dotted trendline is the partial least square regression of the complete core lipid TEX_{86} data set. The solid line marks the 1:1 CL to IPL proxy correspondence indicating both allochthonous and autochthonous sources contribute equally to the core GDGT lipid pool.

3.4. TEX_{86} overprint corrections

The measured TEX_{86} ($_{M}TEX_{86}$) value of the Cathedral Hill sediments is herein considered to be a weighted sum of a sea surface TEX_{86} ($_{SS}TEX_{86}$) value acquired from lipids sourced in the upper water column that is further modified by a component of the deeper water column sourced core lipids ($_{WC}TEX_{86}$) as well as by additions of archaeal lipids from the benthic and subsurface microbial communities ($_{Sed}TEX_{86}$). These ratio loadings are collectively also potentially further modified by diagenetic influences in the ocean bottom

sediments. Over the cumulative sediment burial period and [in consideration of the](#) measured porewater temperatures of the Cathedral Hill push core sediments, these influences include the selective loss of lipids by their binding into protokerogen (K) and [by](#) potential changes due to the loss of lipid by turnover (ϕ ; section 3.1). Additional catagenetic effects from thermochemical alteration of lipids (θ) may also attenuate the sum of sedimentary core lipids by their exposure to high temperature vent fluids. Collectively, these effects are considered to form the following relationship:

$${}_M\text{TEX}_{86} = \frac{a_{SS}\text{TEX}_{86} + b_{WC}\text{TEX}_{86} + c(d_{0-n})_{Sed}\text{TEX}_{86}}{\phi + K + \theta} \quad (7)$$

where a , b , and c , are measured scaling parameters for lipid loading and ϕ , K , and θ are diagenetic and catagenetic alteration parameters. Solving for $SS\text{TEX}_{86}$:

$$SS\text{TEX}_{86} = \frac{{}_M\text{TEX}_{86}(\phi + K + \theta)}{a} - \frac{b_{WC}\text{TEX}_{86} + c(d_{0-n})_{Sed}\text{TEX}_{86}}{a} \quad (8)$$

In this regard, a portion of the archaeal community from the deeper water column, presumably initially sourced of IPLs, and an additional community inhabiting the ocean floor sediments are assumed to eventually die with their respective IPLs gradually becoming converted to CLs that further contribute to the observed ${}_M\text{TEX}_{86}$ value. For this study, no data were collected to calculate $b_{WC}\text{TEX}_{86}$ and its potential impact on ${}_M\text{TEX}_{86}$ is not further considered. However, it is highly likely, given the longer residence times for glycosidic-based headgroups of the identified archaeal IPLs and their relatively short settling time through the water column ([REFs: Lengger et al., 2012](#)) that a component of this lipid source could already be mixed with the $_{Sed}\text{TEX}_{86}$ ~~value-loading~~ ([Lengger et al., 2012](#)). For this study, $_{Sed}\text{TEX}_{86}$ is an IPL- TEX_{86} ratio based on detected 1G-GDGT-1, -2, -3, and Cren' as present in the original paleoclimate proxy (Eq. 1; Table 1; Figure 6). The 2G-GDGT lipids are excluded from the calculation due to their low absolute concentrations ($<2 \mu\text{g/g sed}^{7-1}$), their limited number of detected TEX_{86} core lipid configurations (comprising only of GDGT-1 and GDGT-2; Table A2), and their short stratigraphic zones of occurrence (section 3.1). The $_{Sed}\text{TEX}_{86}$ is further scaled by the summed concentrations of these lipids as they increasingly accumulate with sediment depth (d_{0-n}). ~~For Cathedral Hill,~~ the sum of allochthonous TEX_{86} lipids ($\Sigma[\text{GDGTs}_{CL-\text{TEX}_{86} \text{ lipids}}]_{0-2}$) is estimated to be $120 \mu\text{g/g sed.}$ based on an average surface lipid concentration (0-2 cmbsf) measured across the four core transect. As such,

$$c(d_{0-n}) = \sum_{i=0}^n \left(\frac{[\text{GDGTs}_{IPL-\text{TEX}_{86} \text{ lipids}}]_n}{[\text{GDGTs}_{CL-\text{TEX}_{86} \text{ lipids}}]_{0-2cm}} \right) \quad (9)$$

where n is the deepest point of sediment burial ([further assuming that the surface sediment layer 0-2cmbsf does not having any component of its IPL GDGTs converted to CLs; Table 2](#)).

Selective lipid removal by digenetic and catagenetic processes theoretically may also affect the TEX_{86} value; however, their perspective impact on the directionality and magnitude of the ratio are difficult to predict and equally hard to discretely measure. For Cathedral Hill, although the loss of GDGTs to protokerogen formation could potentially impact the ratio, it has been proven to be very low for the analyze sediments (Bentley et al., [2021-2022](#)). As such, the selectivity of lipid classes being adsorbed to a protokerogen is undeterminable. More importantly, for this site it is insignificant, and the K parameter in Eqs. 7 and 8 is therefore assigned a value of 0.

The degradation rates of each TEX_{86} lipid class were independently measured for the four push cores (Eq. 6; Fig. A2). Given the high geothermal gradient at Cathedral Hill, some of the transect push core sediments resided within zones of active catagenesis (Fig. 2; Dalzell et al., 2021). As the abundance of both CLs and IPLs differentially decreases through the various core sediment profiles with turnover rates that appear to be constrained by porewater temperature changes (section 3.1), the degradation rates must also record the effects of thermochemical oxidative weathering (Fig. 3B). In this case, ϕ and θ are therefore treated as a grouped parameter.

To determine if individual lipid classes were selectively removed during degradation, the variance (s^2) of the rate change as measured from its respective regression slope (i.e. $m_{\log k}$) of the TEX₈₆ lipid classes (Fig. A2; Supplemental Table A3 from Eq. 6) were calculated. For the Cathedral Hill transect, the calculated $m_{\log k}$ s^2 is 0.11, which suggests near equal degradation rates for all TEX₈₆ lipid classes. Therefore, lipid turnover and the concomitant thermochemical oxidation of these lipid classes is also similarly non-selective. A weighing function for the degree of lipid class selectivity during turnover is nonetheless proposed:

$$\varphi + \theta = 1/M\text{TEX}_{86}^{0.11} \quad (10)$$

When applied to Eq. 8 minor changes to the reconstructed lumped $_{SS+WC}\text{TEX}_{86}^H$ ratio are observed consistent with the absence of a comparative relationship between $i\text{GDGT}$ down core lipid depletions and the respective $M\text{TEX}_{86}$ ratios across the biologically active zone of the transect sediments (section 3.1; Figure 3B).

Equation 7 predicts an average transect $_{SS+WC}\text{TEX}_{86}^H$ reconstructed SST of 21.92 ± 0.66 °C with no elevated trends for increasing porewater temperatures across each of the transect cores (Table 2; Figure 6A). The corrected data series show a lack of correlation associated with a near-zero PLS regression slope, suggesting the model backs-out the original SST signal.

If the φ , K , and θ scaling parameters are removed from the calculation the average temperature shifts 2.08 °C lower to 19.69 ± 0.39 °C (Table 2; Figure 6B). The marginal change is likely due to only a few sediment samples displaying evidence of *in situ* hydrocarbon generation associated with thermochemical oxidation (Dalzell et al., 2021). Irrespective of approach, but particularly the case for the more simplified expression, all measures produce values closer to the expected SST of 19.3–20.4 °C that is based on the range of values recorded for core 4 and the three transect surface sediments (section 3.2). These values are ~3 °C lower than the 23–24 °C obtained for the 21-year (1982–2004) satellite-derived MASST data for the Guaymas Basin region (Herrera-Cervantes et al., 2007). Nonetheless, nearly all $M\text{TEX}_{86}$ attenuation can therefore be attributed to sediment microbial overprinting. The high degree of influence is striking given that the upper water flux of GDGTs is estimated to represents up to 93% of the total intact polar and core GDGT lipid pool within these sediments. In this regard, it demonstrated that microbial community influences TEX₈₆ measurements.

The corrected data series show a lack of correlation associated with a near-zero PLS regression slope, suggesting the model backs-out the original SST signal.

Formatted: Font color: Auto, Not Highlight

Formatted: Font color: Auto

Formatted: Font color: Red, Highlight

Formatted: Font color: Red

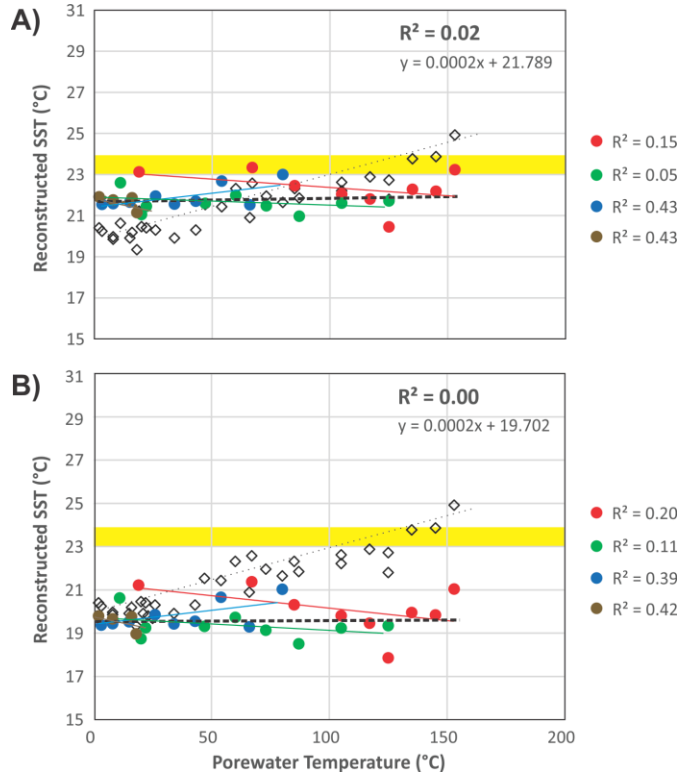


FIGURE 6. Reconstructed $_{ss}TEX_{86}$ SSTs from (A) Eq. 8 and (B) Eq. 8 without ϕ , K , and θ scaling parameters compared to measured porewater temperatures. Red, green, blue, and brown circles indicate recorded values from cores 1, 2, 3, and 4, respectively. $_{ss}TEX_{86}$ values are also plotted for reference (open black diamonds/green circles). Yellow field is the 23–24 °C range observed for the 21-year (1982–2004) satellite-derived MASST data (Herrera-Cervantes et al., 2007). The corrected data series show a lack of correlation suggesting that model can back-out the original SST signal.

706 **Table 2.** Reconstructed sea surface temperatures.
707

Sample	Depth (cmbsf)	Porewater Temp. (°C)	<i>t</i> Time (yrs.)	$M\text{TEX}_{86}$ (Measured iGDGT TEX_{86})	Reconstructed SST (°C)	TEX_{86} 1G- GDGT IPLs ($\mu\text{g/g}^{-1}$)	Cumulative 1G-GDGTs Loading with Depth ($\mu\text{g/g}^{-1}$)	$Sed\text{TEX}_{86}$ (i.e. 1G- GDGT $IPL\text{TEX}_{86}$)	$c(d_{0-n})$ Cumulative Weighted IPL Loading (Eq. 1)
Core 1 (0-2cm)	1	19	10	0.56	21.2	4.80	0	0.58	0.04
Core 1 (2-4cm)	3	67	20	0.58	22.6	3.41	4.80	0.58	0.07
Core 1 (4-6cm)	5	85	30	0.58	22.3	1.29	8.21	0.55	0.08
Core 1 (6-8cm)	7	105	40	0.58	22.2	1.14	9.50	0.57	0.09
Core 1 (8-10cm)	9	117	50	0.59	22.9	1.41	10.64	0.72	0.10
Core 1 (10-12cm)	11	125	60	0.57	21.8	0.76	12.05	0.70	0.11
Core 1 (12-15cm)	13	135	70	0.61	23.8	0.72	12.81	0.69	0.11
Core 1 (15-18cm)	17	145	80	0.61	23.9	0.00	13.53	0.69	0.11
Core 1 (18-21cm)	20	153	90	0.63	24.9	0.00	13.53	0.69	0.11
Avg. Std. Dev.				0.59 0.02	22.84 1.16				
Core 2 (0-2cm)	1	11	10	0.55	20.6	4.33	0	0.46	0.00
Core 2 (2-4cm)	3	22	20	0.54	20.4	1.80	4.33	0.58	0.04
Core 2 (4-6cm)	5	20	30	0.54	20.5	0.76	6.13	0.60	0.05
Core 2 (6-8cm)	7	47	40	0.56	21.5	1.31	6.89	0.71	0.06
Core 2 (8-10cm)	9	60	50	0.58	22.3	0.88	8.20	0.70	0.07
Core 2 (10-12cm)	11	73	60	0.57	22.0	0.92	9.08	0.68	0.08
Core 2 (12-15cm)	13	87	70	0.57	21.8	0.40	10.00	0.73	0.08
Core 2 (15-18cm)	17	105	80	0.58	22.6	0.00	10.40	0.73	0.09
Core 2 (18-21cm)	20	125	90	0.59	22.7	0.00	10.40	0.73	0.09
Avg. Std. Dev.				0.56 0.02	21.61 0.91				
Core 3 (0-2cm)	1	3.2	10	0.54	20.2	3.51	0	0.53	0.03
Core 3 (2-4cm)	3	8	20	0.53	19.9	1.79	3.51	0.49	0.01
Core 3 (4-6cm)	5	15	30	0.53	19.9	1.45	5.30	0.56	0.01
Core 3 (6-8cm)	7	26	40	0.54	20.3	1.77	6.74	0.54	0.01
Core 3 (8-10cm)	9	34	50	0.53	19.9	1.70	8.51	0.61	0.01
Core 3 (10-12cm)	11	43	60	0.54	20.3	2.16	10.21	0.74	0.02
Core 3 (12-15cm)	13	54	70	0.56	21.4	2.52	12.37	0.69	0.02
Core 3 (15-18cm)	17	66	80	0.55	20.9	4.72	14.89	0.74	0.04
Core3 (18-21cm)	20	80	90	0.57	21.6	2.10	19.61	0.66	0.02
Avg. Std. Dev.				0.54 0.01	20.50 0.67				
Core 4 (0-2cm)	1	2	10	0.54	20.4	2.43	0	0.54	0.02
Core 4 (2-4cm)	3	8	20	0.53	20.0	1.75	2.43	0.37	0.01

Core 4 (4-6cm)	5	16	30	0.54	20.2	2.15	4.18	0.43	0.02
Core 4 (6-8cm)	7	18	40	0.52	19.3	1.76	6.34	0.45	0.01
Core 4 (8-10cm)	9	21	50	0.53	19.9	0.44	8.09	-	-
Core 4 (10-12cm)	11	23	60	0.53	19.8	2.20	8.54	-	-
Core 4 (12-15cm)	13	25	70	0.53	19.7	0.00	10.74	-	-
Avg.				0.53	19.90				
Std. Dev.				0.01	0.34				
Avg.									
Std. Dev.									

Table 2. Reconstructed sea surface temperatures (continued).

Sample	Eq. 8 excluding $\phi+0+K$			Eq. 8 including $\phi+0+K$		
	$SS+WC\text{TEX}_{86}^H$ ($M\text{TEX}_{86} - c(d\phi_n)^*_{Sed}\text{TEX}_{86}$)	$SS+WC\text{TEX}_{86}^H$ (after Kim et al., 2010)	$SS+WC\text{TEX}_{86}^H$ Reconstructed SST ($^{\circ}\text{C}$)	$\phi+0$ (Eq. 10) (where $s^2 = 0.11$; Table A3)	$SS+WC\text{TEX}_{86}^H$ Reconstructed SST ($^{\circ}\text{C}$) (after Kim et al., 2010)	$SS+WC\text{TEX}_{86}^H$ Reconstructed SST ($^{\circ}\text{C}$) (after Kim et al., 2010)
Core 1 (0-2cm)	0.56	-0.25	21.2	1.07	0.59	23.1
Core 1 (2-4cm)	0.56	-0.25	21.4	1.07	0.60	23.3
Core 1 (4-6cm)	0.54	-0.27	20.3	1.07	0.58	22.5
Core 1 (6-8cm)	0.53	-0.27	19.8	1.07	0.57	22.0
Core 1 (8-10cm)	0.52	-0.28	19.5	1.07	0.57	21.8
Core 1 (10-12cm)	0.50	-0.30	17.9	1.08	0.54	20.5
Core 1 (12-15cm)	0.53	-0.27	20.0	1.07	0.58	22.3
Core 1 (15-18cm)	0.53	-0.27	19.8	1.07	0.58	22.2
Core 1 (18-21cm)	0.55	-0.26	21.0	1.07	0.60	23.2
Avg.	0.54	-0.27	20.10	1.07	0.58	22.33
Std. Dev.	0.02	0.02	1.08	0.00	0.02	0.89
Core 2 (0-2cm)	0.55	-0.26	20.6	1.07	0.58	22.6
Core 2 (2-4cm)	0.52	-0.28	19.2	1.07	0.56	21.5
Core 2 (4-6cm)	0.51	-0.29	18.7	1.08	0.55	21.1
Core 2 (6-8cm)	0.52	-0.28	19.3	1.07	0.56	21.6
Core 2 (8-10cm)	0.53	-0.28	19.7	1.07	0.57	22.0
Core 2 (10-12cm)	0.52	-0.28	19.1	1.07	0.56	21.5
Core 2 (12-15cm)	0.51	-0.29	18.5	1.08	0.55	21.0
Core 2 (15-18cm)	0.52	-0.28	19.2	1.07	0.56	21.6
Core 2 (18-21cm)	0.52	-0.28	19.3	1.07	0.57	21.7
Avg.	0.52	-0.28	19.32	1.07	0.56	21.61
Std. Dev.	0.01	0.01	0.60	0.00	0.01	0.49
Core 3 (0-2cm)	0.52	-0.28	19.4	1.07	0.56	21.5
Core 3 (2-4cm)	0.52	-0.28	19.4	1.07	0.56	21.6
Core 3 (4-6cm)	0.53	-0.28	19.5	1.07	0.57	21.7
Core 3 (6-8cm)	0.53	-0.27	19.9	1.07	0.57	21.9
Core 3 (8-10cm)	0.52	-0.28	19.4	1.07	0.56	21.6
Core 3 (10-12cm)	0.53	-0.28	19.6	1.07	0.57	21.7
Core 3 (12-15cm)	0.55	-0.26	20.7	1.07	0.59	22.7
Core 3 (15-18cm)	0.52	-0.28	19.3	1.07	0.56	21.5
Core3 (18-21cm)	0.55	-0.26	21.0	1.07	0.59	23.0
Avg.	0.53	-0.27	19.79	1.07	0.57	21.91
Std. Dev.	0.01	0.01	0.62	0.00	0.01	0.55
Core 4 (0-2cm)	0.53	-0.27	19.8	1.07	0.57	21.9
Core 4 (2-4cm)	0.53	-0.28	19.7	1.07	0.57	21.8

Core 4 (4-6cm)	0.53	-0.28	19.8	1.07	0.57	21.9
Core 4 (6-8cm)	0.52	-0.29	19.0	1.08	0.56	21.2
Core 4 (8-10cm)	-	-	-			
Core 4 (10-12cm)	-	-	-			
Core 4 (12-15cm)	-	-	-			
Avg.	0.53	-0.28	19.55	1.07	0.65	21.67
Std. Dev.	0.01	0.01	0.39	0.00	0.01	0.35
			19.71			21.92
			0.79			0.66

708

709

710

711 **4. Conclusions**

712 For this study, we demonstrate the commonly used TEX₈₆ paleoclimate proxy can become heavily impacted
713 by the ocean floor archaeal community. For the Cathedral Hill vent site at Guaymas Basin, the lipids sourced
714 from these sediments resulted in TEX₈₆ reconstructed temperatures that record conditions of the advecting
715 porewaters. However, the impact appears to result from a combination of source inputs, their diagenetic and
716 catagenetic alteration, and further overprint by the additions of lipids from the ocean floor sedimentary
717 archaeal community that has adapted to the high-temperature conditions of the vent fluids by producing more
718 cyclized ring moieties to rigidify their cellular membranes. Together, these processes resulted in absolute
719 TEX₈₆^H temperature offsets of up to 4 °C based on calibrations closely suited to the latitudinal position of
720 Guaymas Basin. Such large offsets could be meaningful to paleoclimate reconstructions (i.e. global changes
721 by 2–4 °C mean completed deglaciation). As such, we further present a method to correct the overprints by
722 both water column and subsurface archaeal community's using IPLs extracted from both of these sources.
723 Although, we have not been able to test this model with lipid inputs from the overlying water column, we
724 have demonstrated its effectiveness at removing sediment sourced overprints, which may not be unique to
725 hydrothermal systems. This approach should be capable of being extended to all near-surface marine sediment
726 systems and may improve the quality of calibration models or climate reconstructions that are based on TEX₈₆
727 measures.

728

729

730 **Conflicts of Interest**

731 The authors declare no conflict of interest.

732

733 **Supplementary information**

734 Supplementary material related to this article can be found on-line at <https://doi.org/.....>

735 **References**

- 736 Bentley, J. N., Ventura, G. T., Dalzell, C. J., Walters, C. C., Peters, C. A., Mennito, A. S., [Nelson, R. K.](#),
737 [Nelson, R. K.](#), Reddy, C. M., Walters, C. J., Seewald, J., & Sievert, S. M. (2021). Archaeal lipid
738 diversity, alteration, preservation at Cathedral Hill, Guaymas Basin, and its link to the deep time
739 preservation paradox. *Organic Geochemistry*. 163:104302.
740 doi.org/10.1016/j.orggeochem.2021.104302. Accepted with revision.
741
742 [Besseling, M., Hopmans, E. C., Koenen, M., van der Meer, M. T. J., Vreugdenhil, S., Schouten, S.,](#)
743

- Sinninghe Damsté, J. S., & Villanueva, L. (2019). Depth-related differences in archaeal populations impact the isoprenoid tetraether lipid composition of the Mediterranean Sea water column. *Organic Geochemistry*, 135, 16–31. doi.org/10.1016/j.orggeochem.2019.06.008.
- Besseling, M. A., Hopmans, E. C., Bale, N. J., Schouten, S., Sinninghe Damsté, J. S., & Villanueva, L. (2020). The absence of intact polar lipid-derived GDGTs in marine waters dominated by Marine Group II: Implications for lipid biosynthesis in Archaea. *Sci Rep* 10, 294. doi.org/10.1038/s41598-019-57035-0.
- Biddle, J. F., Cardman, Z., Mendlovitz, H., Albert, D. B., Lloyd, K. G., Boetius, A., & Teske, A. (2012). ~~Teske, A. (2012).~~ Anaerobic oxidation of methane at different temperature regimes in Guaymas Basin hydrothermal sediments. *The ISME Journal* 6, 1018–1031. <http://dx.doi.org/10.1038/ismej.2011.164> <http://dx.doi.org/10.1038/ismej.2011.164>.
- Boetius, A., Ravenschlag, K., Schubert, C., Rickert, D., Widdel, F., Gieseke, A., Amann, R., Jørgensen, B.B., Witte, U., & Pfannkuche, O. (2000). A marine microbial consortium apparently mediating anaerobic oxidation of methane. *Nature* 407, 623–626. <https://doi.org/10.1038/35036572>.
- Boyd, E., Hamilton, T., Wang, J., He, L., & Zhang, C. (2013). The role of tetraether lipid composition in the adaptation of thermophilic archaea to acidity. *Frontiers in Microbiology*, 4, 62.
- Brochier- Armanet, C., Boussau, B., Gribaldo, S., & Forterre, P. (2008). Mesophilic Crenarchaeota: proposal for a third archaeal phylum, the Thaumarchaeota. *National Review Microbiology* 6, 245–252. doi:10.1038/nrmicro1852. Brassell, S. C., Eglinton, G., Marlowe, I. T., Pflaummann, U., & Sarntin, M. (1986). Molecular stratigraphy: a new tool for climatic assessment. *Nature*, 320, 129–133.
- Calvert, S. E. (1966). Origin of diatom-rich, varved sediments from the Gulf of California. *The Journal of Geology*, 74, 546–565.
- Carr, S. A., Schubotz, F., Dunbar, R. B., Mills, C. T., Dias, R., Summons, R. E., & Mandernack, K. W. (2018). Acetoclastic Methanosaeta are dominant methanogens in organic-rich Antarctic marine sediments. *The ISME Journal*, 12(2), 330–342. <https://doi.org/10.1038/ismej.2017.150>.
- Curry, J. R., Moore, D. G., Lawver, L. A., Emmel, F. J., Raitt, R. W., Henry, M., & Kieckhefer, R. (1979). Tectonics of the Andaman Sea and Burma: convergent margins. In J.S. Watkins, L. Montadert, P.W. Dickerson (Eds.) *Geological and Geophysical Investigations of Continental Margins*, AAPG Memoir 29, 189–198.
- Dalzell, C. J., Ventura, G. T., Nelson, R. K., Reddy, C. M., Walters, C. J., Seewald, J., & Sievert, S. M. (2021). Resolution of multi-molecular hydrocarbon transformation in petroleum-bearing sediments from the Cathedral Hill hydrothermal vent complex at Guaymas Basin, Gulf of California by comprehensive two-dimensional gas chromatography and chemometric analyses. *Journal of Organic Geochemistry*, 152, 104173.
- De Rosa, M., & Gambacorta, A. (1988). The lipids of archaebacteria. *Progress in lipid research*, 27, 153–175.
- Elling, F.J., Könneke, M., Lipp, J.S., Becker, K.W., Gagen, E.J., & Hinrichs, K.-U. (2014). Effects of growth phase on the membrane lipid composition of the thaumarchaeon *Nitrosopumilus maritimus* and their implications for archaeal lipid distributions in the marine environment. *Geochimica et Cosmochimica Acta*, 141, 579–597.

Formatted: Indent: Left: 0.79 cm

Formatted: Not Highlight

Formatted: Default Paragraph Font, Font: 12 pt, English (Canada)

Formatted: Indent: Left: 0 cm, Hanging: 0.75 cm

Formatted: Not Highlight

Formatted: Not Highlight

Formatted: Indent: Left: 0.79 cm, First line: 0 cm

Field Code Changed

Formatted: Default Paragraph Font, Font: 12 pt, Font color: Custom Color(RGB(34,34,34)), Pattern: Clear

Formatted: Not Highlight

Formatted: Indent: Left: 0.8 cm, First line: 0 cm

Formatted: Not Highlight

Formatted: Indent: Left: 0 cm, First line: 0 cm

Formatted: Font: Italic

- Elling, F. J., Könneke, M., Mußmann, M., Greve, A., & Hinrichs, K. U. (2015). Influence of temperature, pH, and salinity on membrane lipid composition and TEX₈₆ of marine planktonic thaumarchaeal isolates. *Geochimica et Cosmochimica Acta*, 171, 238–255.
- Gieskes, J. M., Simoneit, B. R., Brown, T., Shaw, T. J., Wang, Y. C., & Magenheimer, A. (1988). Hydrothermal fluids and petroleum in surface sediments of Guaymas Basin, Gulf of California: a case study. *The Canadian Mineralogist*, 26, 589–602.
- Gliozzi, A., Paoli, G., De Rosa, M., & Gambacorta, A. (1983). Effect of isoprenoid cyclization on the transition temperature of lipids in thermophilic archaeobacteria. *Biochimica et Biophysica Acta (BBA)-Biomembranes*, 735, 234–242.
- Herrera-Cervantes, H., Lluch-Cota, D. B., Lluch-Cota, S. E., & Gutiérrez-de-Velasco, S. G. (2007). The ENSO signature in sea-surface temperature in the Gulf of California. *Journal of Marine Research*, 65, 589–605. doi.org/10.1357/002224007783649529.
- Herfort, L., Schouten, S., Boon, J. P. & Sinninghe Damsté, J. S. (2006). Application of the TEX₈₆ temperature proxy to the southern North Sea. *Organic Geochemistry* 37, 1715–26.
- Ho, S. L. & Laepple, T. (2016). Flat meridional temperature gradient in the early Eocene in the subsurface rather than surface ocean. *Nature Geoscience*, 9, 606–610.
- Hollis, C.J., Taylor, K.W.R., Handley, L., Pancost, R.D., Huber, M., Creech, J.B., Hines, B.R., Crouch, E.M., Morgans, H.E.G., Crampton, J.S., Gibbs, S., Pearson, P.N., & Zachos, J.C. (2012). Early Paleogene temperature history of the Southwest Pacific Ocean: Reconciling proxies and models. *Earth and Planetary Science Letters* 349–350, 53–66
- Hopmans, E. C., Weijers, J. W., Schefuß, E., Herfort, L., Sinninghe Damsté, J. S., & Schouten, S. (2004). A novel proxy for terrestrial organic matter in sediments based on branched and isoprenoid tetraether lipids. *Earth and Planetary Science Letters*, 224, 107–116.
- Huguet, C., Cartes, J. E., Sinninghe Damsté, J. S., & Schouten, S. (2006). Marine crenarchaeotal membrane lipids in decapods: Implications for the TEX₈₆ paleothermometer. *Geochemistry, Geophysics, Geosystems*, 7. doi 10.1029/2006GC001305.
- Huguet, C., Martrat, B., Grimalt, J. O., Sinninghe Damsté, J. S. & Schouten, S. (2011). Coherent millennial-scale patterns in U37 k0 and TEX₈₆ H temperature records during the penultimate interglacial-to-glacial cycle in the western Mediterranean. *Paleoceanography* 26. DOI: 10.1029/2010PA002048.
- Huguet, C., Schimmelmann, A., Thunell, R., Lourens, L. J., Sinninghe Damsté, J. S., & Schouten, S. (2007). A study of the TEX₈₆ paleothermometer in the water column and sediments of the Santa Barbara Basin, California. *Paleoceanography*, 22. doi 10.1029/2006PA001310.
- Hurley, S.J., Elling, F.J., Könneke, M., Buchwald, C., Wankel, S.D., Santoro, A.E., Lipp, J.S., Hinrichs, K.-U., Pearson, A., (2016). Influence of ammonia oxidation rate on thaumarchaeal lipid composition and the TEX₈₆ temperature proxy. *Proceedings of the National Academy of Sciences, U. S. A.*, 113, 7762–7767.
- Kallmeyer, J., & Boetius, A. (2004). Effects of temperature and pressure on sulfate reduction and anaerobic oxidation of methane in hydrothermal sediments of Guaymas Basin. *Applied and Environmental Microbiology*. 70, 1231–1233. doi.org/10.1128/AEM.70.2.1231-1233.2004.
- Karner, M. B., DeLong, E. F., Karl, D. M. (2001). Archaeal dominance in the mesopelagic zone of the Pacific Ocean. *Nature*. 25, 409(6819), 507–510. doi: 10.1038/35054051.

Formatted: Not Highlight

Formatted: Not Highlight

Formatted: Not Highlight

Formatted: Not Highlight

Formatted: Indent: Left: 0.8 cm

Formatted: Not Highlight

Formatted: Not Highlight

Formatted: Not Highlight

Formatted: Not Highlight

Formatted: Not Highlight

Formatted: Not Highlight

Formatted: Indent: Left: 0 cm, First line: 0 cm

Formatted: Not Highlight

Formatted: Not Highlight

Formatted: Not Highlight

Formatted: Not Highlight

Formatted: Not Highlight

Formatted: Not Highlight

Formatted: Not Highlight

Formatted: Not Highlight

Formatted: Not Highlight

Formatted: Not Highlight

Formatted: Not Highlight

Formatted: Indent: Left: 0 cm, First line: 0 cm

Formatted: Not Highlight

- Kashefi, K., & Lovley, D. R. (2003). Extending the upper temperature limit for life. *Science*, 301, 934–934.
- Kim, J. H., Schouten, S., Hopmans, E. C., Donner, B., & Damsté, J. S. S. (2008). Global sediment core-top calibration of the TEX₈₆ paleothermometer in the ocean. *Geochimica et Cosmochimica Acta*, 72, 1154–1173.
- Kim, J. H., Van der Meer, J., Schouten, S., Helmke, P., Willmott, V., Sangiorgi, F., Koç, N., Hopmans, E. C. & Damsté, J. S. S. (2010). New indices and calibrations derived from the distribution of crenarchaeal isoprenoid tetraether lipids: Implications for past sea surface temperature reconstructions. *Geochimica et Cosmochimica Acta*, 74, 4639–4654.
- Kim J.-H., Romero O. E., Lohmann G., Donner B., Laepple T., Haam E. & Sinninghe Damsté J. S. (2012a) Pronounced subsurface cooling of North Atlantic waters off Northwest Africa during Dansgaard-Oeschger interstadials. *Earth and Planetary Science Letters*, 339–340, 95–102.
- Kim, J. H., Crosta, X., Willmott, V., Renssen, H., Bonnin, J., Helmke, P., Schouten, S. & Sinninghe Damsté, J. S. (2012b). Holocene subsurface temperature variability in the eastern Antarctic continental margin. *Geophysical Research Letters*, 39. doi 10.1029/2012GL051157.
- Kim J.-H., Schouten, S., Rodrigo-Gamiz, M., Rampen, S., Marino, G., Huguet, C., Helmke, P., Buscail, R., Hopmans, E. C., Pross, J., Sangiorgi, F., Middelburg, J. B. M., & Sinninghe Damsté J. S. (2015). Influence of deep-water derived isoprenoid tetraether lipids on the paleothermometer in the Mediterranean Sea. *Geochimica et Cosmochimica Acta*, 150, 125–141.
- Knappy, C. S., Chong, J. P., & Keely, B. J. (2009). Rapid discrimination of archaeal tetraether lipid cores by liquid chromatography-tandem mass spectrometry. *Journal of the American Society for Mass Spectrometry*, 20, 51–59.
- [Kumar, D. M., Woltering, M., Hopmans, E. C., Sinninghe Damsté, J. S., Schouten, S. & Werne, J. P. \(2019\). The vertical distribution of Thaumarchaeota in the water column of Lake Malawi inferred from core and intact polar tetraether lipids. *Organic Geochemistry* 132, 37-49.](#)
- Lawrence, K. T., Pearson, A., Castaneda, I. S., Ladow, C., Peterson, L. C., Lawrence, G. E. (2020). Comparison of Late Neogene U^k₃₇ and TEX₈₆ Paleotemperature records from the eastern equatorial Pacific at orbital resolution. *Paleoceanography and Paleoclimatology*, 35, 1–16.
- Lengger, S.K., Hopmans, E.C., Reichart, G.-J., Nierop, K.G.J., Sinninghe Damsté, J.S., Schouten, S. (2012). Intact polar and core glycerol dibiphytanyl glycerol tetraether lipids in the Arabian Sea oxygen minimum zone. Part II: Selective preservation and degradation in sediments and consequences for the TEX₈₆. *Geochimica et Cosmochimica Acta* 98, 244–258.
- [Lengger, S. K., Hopmans, E. C., Sinninghe Damsté, J. S., Schouten, S. \(2014\). Fossilization and degradation of archaeal intact polar tetraether lipids in deeply buried marine sediments \(Peru Margin\). *Geobiology*, 12\(3\), 212–220, <https://doi.org/10.1111/gbi.12081>.](#)
- [Lincoln, S. A., Wai, B., Eppley, J. M., Church, M. J., Summons, R. E., & DeLong, E. F. \(2014\). Planktonic euryarchaeota are a significant source of archaeal tetraether lipids in the ocean. *Proceedings of the National Academy of Sciences, U. S. A.* 111, 9858–9863. doi: 10.1073/pnas.1409439111.](#)
- [Lipp, J. S., & Hinrichs, K. U. \(2009\). Structural diversity and fate of intact polar lipids in marine sediments. *Geochimica et Cosmochimica Acta*, 73, 6816–6833.](#)

Formatted: Not Highlight

Formatted: Indent: Left: 0 cm, First line: 0 cm

Formatted: Not Highlight

Formatted: Not Highlight

Formatted: Not Highlight

Formatted: Not Highlight

Formatted: Indent: Left: 0 cm, First line: 0 cm

Formatted: Not Highlight

Formatted: Not Highlight

Formatted: Not Highlight

Formatted: Indent: Left: 0 cm, First line: 0 cm

- Lipp, J. S., Morono, Y., Inagaki, F., & Hinrichs, K. U. (2008). Significant contribution of Archaea to extant biomass in marine subsurface sediments. *Nature*, 454, 991–994.
- Li, D., Zhang, C. L., (2017). Marine Group II Dominant Benthic Archaea in Water Column of the Northeastern South China Sea.
- Liu, X. L., Leider, A., Gillespie, A., Gröger, J., Versteegh, G. J., & Hinrichs, K. U. (2010). Identification of polar lipid precursors of the ubiquitous branched GDGT orphan lipids in a peat bog in Northern Germany. *Organic Geochemistry*, 41, 653–660.
- Liu, X. -L., Lipp, J. S., Hinrichs, K. -U. (2011). Distribution of core and intact GDGTs in marine sediments. *Organic Geochemistry* 42, 368–375.
- Liu, X. -L., Lipp, J. S., Simpson, J. H., Lin, Y. S., Summons, R. E., & Hinrichs, K. U. (2012). Mono and dihydroxyl glycerol dibiphytanyl glycerol tetraethers in marine sediments: Identification of both core and intact polar lipid forms. *Geochimica et Cosmochimica Acta*, 89, 102–115.
- Liu, X. L., Russell, D. A., Bonfio, C., Summons, R. E. (2018) Glycerol configurations of environmental GDGTs investigated using a selective sn2 ether cleavage protocol. *Organic Geochemistry*, 128, 57–62.
- Lipp, J. S., & Hinrichs, K. U. (2009). Structural diversity and fate of intact polar lipids in marine sediments. *Geochimica et Cosmochimica Acta*, 73, 6816–6833.
- Lipp, J. S., Morono, Y., Inagaki, F., & Hinrichs, K. U. (2008). Significant contribution of Archaea to extant biomass in marine subsurface sediments. *Nature*, 454, 991–994.
- Lonsdale, P., & Becker, K. (1985). Hydrothermal plumes, hot springs, and conductive heat flow in the Southern Trough of Guaymas Basin. *Earth and Planetary Science Letters*, 73, 211–225.
- Lopes dos Santos R. A., Prange M., Castaneda I. S., Schefuß E., Mulitza S., Schulz M., Niedermeyer E. M., Sinninghe Damsté J. S. and Schouten S. (2010). Glacial–interglacial variability in Atlantic meridional overturning circulation and thermocline adjustments in the tropical North Atlantic. *Earth and Planetary Science Letters*, 300, 407–414.
- Lunt, D. J., Haywood, A. M., Schmidt, G. A., Salzmann, U., Valdes, P. J., Dowsett, H. J., & Loptson, C.A. (2012). On the causes of mid-Pliocene warmth and polar amplification. *Earth and Planetary Science Letters*, 321–322, 128–138, doi:10.1016/j.epsl.2011.12.042.
- Ma, C., Coffinet, S., Lipp, J. S., Hinrichs, K. U., & Zhang, C. (2020). Marine Group II Euryarchaeota Contribute to the Archaeal Lipid Pool in Northwestern Pacific Ocean Surface Waters. *Frontiers in microbiology*, 11, 1034. <https://doi.org/10.3389/fmicb.2020.01034>.
- Macalady, J. L., Vestling, M. M., Baumler, D., Boekelheide, N., Kaspar, C. W., & Banfield, J. F. (2004). Tetraether-linked membrane monolayers in *Ferroplasma* spp: a key to survival in acid. *Extremophiles*, 8, 411–419.
- McClymont, E. L., Ganeshram, R. S., Pichevin, L. E., Talbot, H. M., van Dongen, B. E., Thunell, R. C., Haywood, A.M., Singarayer, J.S. & Valdes, P. J. (2012). Sea-surface temperature records of Termination 1 in the Gulf of California: Challenges for seasonal and interannual analogues of tropical Pacific climate change. *Paleoceanography*, 27. doi 10.1029/2011PA002226.
- McKay, L. J., MacGregor, B. J., Biddle, J. F., Albert, D. B., Mendlovitz, H. P., Hoer, D. R., Lipp, J.S., Lloyd, K.G & Teske, A. P. (2012). Spatial heterogeneity and underlying geochemistry of phylogenetically diverse orange and white Beggiatoa mats in Guaymas Basin hydrothermal sediments. *Deep Sea Research Part I: Oceanographic Research Papers*, 67, 21–31.

Formatted: Highlight

Formatted: Indent: Left: 0 cm, First line: 0 cm

965 Meyer, S., Wegener, G., Lloyd, K. G., Teske, A., Boetius, A., & Ramette, A. (2013). Microbial habitat
 966 connectivity across spatial scales and hydrothermal temperature gradients at Guaymas
 967 Basin. *Frontiers in Microbiology*, 4, 207.
 968
 969 [Moore, D. G. \(1973\). Plate edge deformation and crustal growth, Gulf of California structural
 970 province. *Geological Society of America Bulletin*, 84, 1883–1906.](#)
 971
 972 [Morrisey, A., Scholz, C.A., & Russell, J.M. \(2018\). Late Quaternary TEX₈₆ paleotemperatures from the
 973 world's largest desert lake, Lake Turkana, Kenya. *Journal of Paleolimnology* 59, 103–117.](#)
 974
 975 Naafs, B. D. A., Rohrsen, M., Inglis, G. N., Lähenteenoja, O., Feakins, S. J., Collinson, M. E., Kennedy,
 976 E.M., Singh, P.K., Singh, M.P., Lunt, D.J., & Pancost, R. D. (2018). High temperatures in the
 977 terrestrial mid-latitudes during the early Palaeogene. *Nature Geoscience*, 11, 766–771.
 978
 979 [O'Brien, C.L., Robinson, S.A. Pancost, R.D., Sinninghe Damste, J.S., Schouten, S., Lunt, D.J., Alsenz, H.,
 980 Bomemann, A., Bottini, C., Brassell, S.C., Farnsworth, A., Forster, A., Huber, B.T., Inglis, G.N.,
 981 Jenkyns, H.C., Linnert, C., Littler, K., Markwick, P., McAnena, A., Mutterlose, J., Naafs, B.D.A.,
 982 Puttmann, W., Sluijs, A., van Helmond, N.A.G.M., Vellekoop, J., Wagner, T., & Wrobel, N.E.
 983 \(2017\). Cretaceous sea-surface temperature evolution: Constraints from TEX₈₆ and planktonic
 984 foraminiferal oxygen isotopes. *Earth-Science Reviews*. 172, 224–247.](#)
 985
 986
 987
 988 Pearson, A. and Ingalls, A. E. (2013) Assessing the use of archaeal lipids as marine environmental
 989 proxies.
 990 *Annual Review Earth Planetary Science*. 41, 15.1–15.26.
 991
 992 Pearson, A., Huang, Z., Ingalls, A. E., Romanek, C. S., Wiegel, J., Freeman, K. H., Smittenberg, R. H. &
 993 Zhang, C. L. (2004). Nonmarine crenarchaeol in Nevada hot springs. *Applied and Environmental*
 994 *Microbiology*, 70, 5229–5237.
 995
 996 [Petrick, B., Reuning, L., & Martinez-Garcia \(2019\) Distribution of Glycerol Dialkyl Glycerol Tetraethers
 997 \(GDGTs\) in Microbial Mats From Holocene and Miocene Sabkha Sediments. *Frontiers in Earth*
 998 *Science*. 04. doi.org/10.3389/feart.2019.00310.](#)
 999
 1000 Powers, L., Werne, J. P., Vanderwoude, A. J., Sinninghe Damsté, J. S., Hopmans, E. C., & Schouten, S.
 1001 (2010). Applicability and calibration of the TEX₈₆ paleothermometer in lakes. *Organic*
 1002 *Geochemistry*, 41, 404–413.
 1003
 1004 Qin, W., Carlson, L. T., Armbrust, E. V., Devol, A. H., Moffett, J. W., Stahl, D. A., & Ingalls, A. E. (2015).
 1005 Confounding effects of oxygen and temperature on the TEX₈₆ signature of marine Thaumarchaeota.
 1006 *Proceedings of the National Academy of Sciences*, [U. S. A.](#) 112(35), 10.979–10.984.
 1007 [https://doi.org/10.1073/pnas.1501568112doi.org/10.1073/pnas.1501568112.](#)
 1008
 1009 [Robinson, S. A., Ruhl, M., Astley, D. L., Naafs, B. D. A., Farnsworth, A. J., Bown, P. R., Jenkyns, H. C.,
 1010 Lunt, D. J., O'Brien, C., Pancost, R. D., & Markwick, P. J. \(2017\). Early Jurassic North Atlantic sea-
 1011 surface temperatures from TEX₈₆. *Palaeothermometry. Sedimentology*. 64, 215–230.](#)
 1012
 1013 [Rommerskirchen, F., Condon, T., Mollenhauer, G., Dupont, L. M., & Schefuß, E. \(2011\). Miocene to
 1014 Pliocene development of surface and subsurface temperatures in the Benguela Current system.
 1015 *Paleoceanography*, 26, PA3216, 1-15. doi.org/10.1029/2010PA002074.](#)
 1016
 1017 Schouten, S., Hopmans, E. C., and Sinninghe Damsté, J. S. (2013). The organic geochemistry of glycerol
 1018 dialkyl glycerol tetraether lipids: A review. *Organic Geochemistry*, 54, 19–61.
 1019
 1020

Formatted: Subscript

Formatted: Not Highlight

Formatted: Not Highlight

Formatted: Not Highlight

Formatted: Indent: Left: 0 cm, First line: 0 cm

Formatted: Not Highlight

Formatted: Not Highlight

Formatted: Not Highlight

Formatted: Subscript

Formatted: Not Highlight

Formatted: Default Paragraph Font, Font: 12 pt, Pattern: Clear

Formatted: Indent: Left: 0 cm, First line: 0 cm

Formatted: Indent: Left: 0.75 cm, First line: 0 cm

Formatted: Not Highlight

Formatted: Indent: Left: 0 cm, First line: 0 cm

Formatted: Not Highlight

- Schouten, S., Hopmans, E. C., & Sinninghe Damsté, J. S. (2004). The effect of maturity and depositional redox conditions on archaeal tetraether lipid palaeothermometry. *Organic Geochemistry*, 35, 567–571.
- Schouten, S., Hopmans, E. C., Schefuß, E., & Sinninghe Damsté, J. S. (2002). Distributional variations in marine crenarchaeotal membrane lipids: a new tool for reconstructing ancient sea water temperatures? *Earth and Planetary Science Letters*, 204, 265–274.
- Schouten S., Wakeham S. G., Hopmans E. C. and Sinninghe Damsté J. S. (2003) Biogeochemical Evidence that Thermophilic Archaea Mediate the Anaerobic Oxidation of Methane. *Appl. Environ. Microbiol.* 69, 1680–1686.
- Seki, O., Bendle, J. A., Haranda, N., Kobayashi, M., Sawada, K., Moossen, H., Inglis, G. N., Nagao, S., & Sakamoto, T. (2014). Assessment and calibration of TEX₈₆ paleothermometry in the Sea of Okhotsk and sub-polar North Pacific region: Implications for paleoceanography. *Progress in Oceanography*, 126, 254–266.
- Sinninghe Damsté, J. S., Ossebaer, J., Abbas, B., Schouten, S., & Verschuren, D. (2009). Fluxes and distribution of tetraether lipids in an equatorial African lake: constraints on the application of the TEX₈₆ palaeothermometer and BIT index in lacustrine settings. *Geochimica et Cosmochimica Acta*, 73, 4232–4249.
- Sinninghe Damsté J. S., Rijpstra W. I. C., Hopmans E. C., den Uijl M. J., Weijers J. W. H. and Schouten S. (2018) The enigmatic structure of the crenarchaeol isomer. *Organic Geochemistry* 124, 22–28.
- Stadnitskaia, A., Nadezhkin, D., Abbas, B., Blinova, V., Ivanov, M. K., & Sinninghe Damsté, J. S. (2008). Carbonate formation by anaerobic oxidation of methane: evidence from lipid biomarker and fossil 16S rDNA. *Geochimica et Cosmochimica Acta*, 72(7), 1824–1836.
- Sturt, H. F., Summons, R. E., Smith, K., Elvert, M., & Hinrichs, K. U. (2004). Intact polar membrane lipids in prokaryotes and sediments deciphered by high-performance liquid chromatography/electrospray ionization multistage mass spectrometry—new biomarkers for biogeochemistry and microbial ecology. *Rapid communications in mass spectrometry*, 18, 617–628.
- Teske, A., Callaghan, A. V., & LaRowe, D. E. (2014). Biosphere frontiers of subsurface life in the sedimented hydrothermal system of Guaymas Basin. *Frontiers in Microbiology*, 5, 362.
- Teske, A., De Beer, D., McKay, L. J., Tivey, M. K., Biddle, J. F., Hoer, D., Lloyd, K. G., Lever, M. A., Røy, H., Albert, D. B. & MacGregor, B. J. (2016). The Guaymas Basin hiking guide to hydrothermal mounds, chimneys, and microbial mats: Complex seafloor expressions of subsurface hydrothermal circulation. *Frontiers in Microbiology*, 7, 75.
- Tierney, J. E. (2014). Biomarker-based inferences of past climate: the TEX₈₆ paleotemperature proxy. In H. D. Holland & K. K. Turekian (Eds.) *Treatise on Geochemistry* (2nd Ed.) 12, 379–939.
- Uda, I., Sugai, A., Itoh, Y. H., & Itoh, T. (2001). Variation in molecular species of polar lipids from *Thermoplasma acidophilum* depends on growth temperature. *Lipids*, 36, 103–105.
- Umoh, U., Li L., Luckge, A., Schwartz-Schampera, U., & Naafs, D. (2020). Influence of hydrothermal vent activity on GDGT pool in marine sediments might be less than previously thought. *Organic Geochemistry*. 104102. doi.org/10.1016/j.orggeochem.2020.104102.
- Wakeham, S. G., Lewis, C. M., Hopmans, E. C., Schouten, S., & Sinninghe Damsté, J. S. (2003). Archaea mediate anaerobic oxidation of methane in deep euxinic waters of the Black Sea. *Geochimica et Cosmochimica Acta*, 67, 1359–1374.

Formatted: Font: Not Italic

Formatted: Not Highlight

Formatted: Not Highlight

Formatted: Subscript

Formatted: Not Highlight

Formatted: Font: Font color: Custom Color(RGB(0,0,10)), (Asian) Chinese (China), Pattern: Clear, Not Highlight

Formatted: Not Highlight

Formatted: Indent: Left: 0 cm, First line: 0 cm

Formatted: Not Highlight

Formatted: Indent: Left: 0 cm, First line: 0 cm

Formatted: Not Highlight

Formatted: Not Highlight

- 1077 Wang, J. X., Wei, Y., Wang, P., Hong, Y., & Zhang, C. L. (2015). Unusually low TEX₈₆ values in the
1078 transitional zone between Pearl River estuary and coastal South China Sea: impact of changing
1079 archaeal community composition. *Chemical Geology*, 402, 18–29. doi:
1080 10.1016/j.chemgeo.2015.03.002
- 1081
- 1082 Weijers, J. W., Schefuß, E., Kim, J. H., Sinninghe Damsté, J. S., & Schouten, S. (2014). Constraints on the
1083 sources of branched tetraether membrane lipids in distal marine sediments. *Organic Geochemistry*, 72,
1084 14–22.
- 1085
- 1086 Weijers, J. W., Schouten, S., van den Donker, J. C., Hopmans, E. C., & Sinninghe Damsté, J. S. (2007).
1087 Environmental controls on bacterial tetraether membrane lipid distribution in soils. *Geochimica et*
1088 *Cosmochimica Acta*, 71, 703–713.
- 1089
- 1090 Wuchter, C., Schouten, S., Wakeham, S. G., & Sinninghe Damsté, J. S. (2005). Temporal and spatial
1091 variation in tetraether membrane lipids of marine Crenarchaeota in particulate organic matter:
1092 Implications for TEX₈₆ paleothermometry. *Paleoceanography*, 20, doi 10.1029/2004PA001110.
- 1093
- 1094 Wuchter, C., Schouten, S., Wakeham, S. G., & Sinninghe Damsté, J. S. (2006). Archaeal tetraether
1095 membrane lipid fluxes in the northeastern Pacific and the Arabian Sea: implications for TEX₈₆
1096 paleothermometry. *Paleoceanography* 21.
- 1097
- 1098 Yao, Y., Zhao, J., Bauersachs, T., & Huang, Y. (2019). Effect of water depth on the TEX₈₆ proxy in
1099 volcanic lakes of northeastern China. *Organic Geochemistry* 129, 88–89.
- 1100
- 1101 Yoshinaga, M. Y., Kellermann, M. Y., Rossel, P. E., Schubotz, F., Lipp, J. S., & Hinrichs, K. U. (2011).
1102 Systematic fragmentation patterns of archaeal intact polar lipids by high-performance liquid
1103 chromatography/electrospray ionization ion-trap mass spectrometry. *Rapid Communications in Mass*
1104 *Spectrometry*, 25, 3563–3574.
- 1105
- 1106 Zeng, Z., Liu, X. L., Farley, K. R., Wei, J. H., Metcalf, W. W., Summons, R. E., & Zhang, Y. G., Pagani,
1107 M., & Wang, Z. (2016). Ring Index: A new strategy to evaluate the integrity of TEX₈₆
1108 paleothermometry. *Paleoceanography*, 31, 220–232.
- 1109
- 1110 Zhang, Y. G., Zhang, C. L., Liu, X. L., Li, L., Hinrichs, K. U., & Noakes, J. E. (2011). Methane Index: A
1111 tetraether archaeal lipid biomarker indicator for detecting the instability of marine gas hydrates. *Earth*
1112 *and Planetary Science Letters*, 307, 525–534.
- 1113
- 1114 Zhang, Y. G., Pagani, M. & Wang, Z. (2016). Ring Index: A new strategy to evaluate the integrity of
1115 TEX₈₆ paleothermometry. *Paleoceanography and Paleoclimatology* 31:220–232, doi.org/
1116 10.1002/2015PA002848.
- 1117
- 1118
- 1119 Zhu, C., Lipp, J. S., Wörmer, L., Becker, K. W., Schröder, J., & Hinrichs, K. U. (2013). Comprehensive
1120 glycerol ether lipid fingerprints through a novel reversed phase liquid chromatography–mass
1121 spectrometry protocol. *Organic Geochemistry*, 65, 53–62.

Formatted: Not Highlight

Formatted: Subscript

Formatted: Not Highlight

Formatted: Not Highlight

Formatted: Subscript

Formatted: Not Highlight

Formatted: Indent: First line: 0 cm

Formatted: Not Highlight